

Article citation info:

Zhao Z, Xie L, Zhao B, Wang L, Reliability assessment of folding wing system deployment performance considering failure correlation, *Eksploracja i Niezawodność – Maintenance and Reliability* 2024; 26(1) <http://doi.org/10.17531/ein/175085>

Reliability assessment of folding wing system deployment performance considering failure correlation

Indexed by:



Zhiqiang Zhao^{a, b}, Liyang Xie^{a, b, *}, Bingfeng Zhao^{a, b}, Lei Wang^c

^a School of Mechanical Engineering & Automation, Northeastern University, Shenyang 110819, P. R. China

^b Key Laboratory of Vibration and Control of Aero-Propulsion System Ministry of Education, Shenyang 110819, P. R. China

^c School of Mechanical Engineering, Suzhou University of Science and Technology, Suzhou 215009, P. R. China

Highlights

- Dynamic model of the folding wing mechanism with joint clearances is developed and solved.
- The system reliability models with failure correlation are established.
- The new evaluation methods for the system reliability models are proposed.
- Variation rules of system reliability with different distribution parameters are analyzed.

Abstract

The reliability of folding wing deployment performance greatly impacts flight vehicle reliability. Based on the dynamic analysis theory, the deployment dynamic model of folding wing mechanism with joint clearances is established and solved. Considering the failure correlation, the system reliability models are developed for both cases, without considering synchronization and considering synchronization. For the former, a solution method combining saddle point approximation and numerical integration is proposed. For the latter, an estimation method based on a combination of the fourth order moment Pearson distribution family and the numerical integration is proposed. The efficiency and accuracy of the proposed methods are verified through examples. In addition, the trend of the system reliability change when the distribution parameters of random variables are different is also analyzed. From the perspective of improving reliability, the above study can provide theoretical guidance and data support for the design, manufacturing and service process of the folding wing mechanism system.

Keywords

folding wing mechanism, deployment performance, failure correlation, system reliability, reliability assessment.

This is an open access article under the CC BY license (<https://creativecommons.org/licenses/by/4.0/>)

1. Introduction

As a vital flight control unit, the folding wing mechanism ensures flight safety, stability, and trajectory adjustments. Its deployment performance reliability directly impacts the flight vehicle's mission success. Therefore, it is necessary to evaluate the reliability of the deployment performance of the folding wing system.

Generally, successful deployment is achieved when the mechanism's deployment time remains under a threshold. In harsh environments, this also involves synchronization

reliability, where the time span between maximum and minimum deployment must stay below a threshold. These reliability indicators are related to the deployment time, so the dynamic of the folding wing mechanism with clearances needs to be modeled and solved. Many scholars have studied the dynamics of planar multibody systems containing joint clearances. Flores et al. 10,11 examined contact forces in revolute joints with clearances, and solved a crank-slider mechanism dynamic model using numerical integration. Mukras et al. 28 deduced hinge wear depth variation after long-term operation. Zheng et al. 43 built a dynamic model for a

(*) Corresponding author.

E-mail addresses:

Z. Zhao (ORCID: 0009-0008-7619-0126) 18245143082@163.com, L. Xie (ORCID: 0000-0003-4573-0317) lyxieneu@163.com, B. Zhao (ORCID: 0000-0002-6752-0284) 15940488242@163.com, L. Wang (ORCID: 0000-0003-3546-0990) leiwang@sau.edu.cn

flexible multilink high-speed press with joint clearance. Li et al. 23,24 focused on deployment mechanisms. They developed a model for rigid-flexible solar sail system dynamics with joint clearances. Li et al. 21 simulated spatial deployment mechanisms, studying the impacts of clearance, damping, friction, gravity, and flexibility on dynamic performance. These studies offer valuable insights for establishing and solving dynamic models for folding wing mechanisms with clearances.

Traditional series system reliability calculation involves the assumption of independent component failures. However, in complex engineering scenarios, component failures often exhibit statistical correlation, which makes the independence assumption of traditional models invalid. Failure correlation was first proposed by Epler and has been studied in depth by many scholars. Marshall et al. 26 first proposed a multidimensional exponential distribution model, which is the basis for many subsequent failure correlation analysis models. Fleming 9 proposed the β factor model, which has the advantages of few parameters, simplicity and flexibility. However, this model is only applicable to second-order redundant systems. Vaurio et al. 31 proposed the basic parameter (BP) model, which can be applied to calculate the failure probability of each order directly from the known failure data. Fleming et al. 8 proposed the Multiple Greek Letter (MGL) model on the basis of the β factor model, which is widely used in failure correlation analysis. Mosleh et al. 27 proposed the α factor model, which is more accurate than the β factor model. Currently, polynomial multilevel binomial failure rate 15 and parametric mixture 18 models are also proposed for failure correlation analysis. Zhang et al. 38 proposed a unit conditional probability based on safety, failure, and hybrid information to approximate the reliability calculation problem for series, parallel, and voting systems when considering failure correlation. Although the above methods are able to deal with the failure correlation problem, they fail to deeply analyze the causes of system failure correlation and the interaction law. Xie et al. 35 proposed a system-level load-strength interference model, which not only avoids the assumption of "failure independence", but also does not rely on the correlation coefficient. This research can provide a theoretical basis for the establishment of reliability models for similar engineering systems.

At present, many reliability evaluation methods have been derived for various reliability problems. Monte Carlo simulation (MCS) is the most classical and widely used numerical simulation method 13,22. Zhuang et al. 48 applied MCS to obtain the dynamic wear reliability of aircraft locking mechanism. However, the efficiency of MCS is difficult to be accepted when dealing with time-consuming engineering simulations (multibody system dynamics). The first-order reliability method (FORM) 5,14 is very efficient. But FORM will have large errors when dealing with high nonlinear problems. In order to balance the efficiency and accuracy of reliability evaluation, the response surface method 3,36 has been proposed. Support vector machine 17,39 has also been widely used in reliability assessment. The nonlinear fitting capability of artificial neural networks is also strong, so they can also be used in surrogate models 7,44. The Kriging model 33,34 also has a good fitting effect on the problems of high nonlinearity and local response mutation. The maximum entropy method 19,20,47 is a method to approximate the output response probability density function. The saddle point approximation (SPA) method 4,45 can solve the probability density function (PDF) of the output response quickly and accurately. In addition, the hybrid dimension reduction method 37 can still analyze the mechanism reliability. The Pearson frequency curve method based on the first four moment is to approximate the PDF by the Pearson distribution family 25,40,41,42. All these types of methods mentioned above have achieved good results in different reliability problems.

Currently, the majority of research centers on the dynamic attributes of deployment mechanisms, with limited attention to their reliability evaluation. Fewer still delve into the reliability assessment of folding wing deployment mechanisms. Gao et al. 12 analyzed the reliability of deployment synchronization. However, this study does not consider not only the mechanism joint clearance but also the failure correlation under external random aerodynamic loads. Pang et al. 29 calculated the deployment performance and impact resistance reliability of the folding tail system by the response surface method and MCS. However, the influence of joint clearance and the number of deployments are not considered. Pang et al. 30 also conducted an in-depth study on the synchronization reliability. But this method does not consider the correlation caused by load-sharing

characteristics. Wang et al. 32 considered the failure correlation of the folding wing system and solved the deployment reliability through a system-level load-strength interference model. Nonetheless, this study did not analyze the synchronization, and the conditional deployment time distribution assumed normal, limiting applicability.

To comprehensively address the shortcomings of the above studies and to improve the computational efficiency as much as possible in the reliability assessment process, we took the folding wing deployment mechanism as the object of this study, and conducted an in-depth study on the reliability assessment process including failure correlation by taking into full consideration the problems that have not been considered in the above studies. In addition, to the best of our knowledge, there is no systematic report on the reliability assessment of deployment time and deployment synchronization of the folding wing system with clearance considering failure correlation, which is also the purpose of this study. In this study, we considered failure correlation due to external random loads and joint clearances in the folding wing system. The deployment time reliability and the deployment synchronization reliability with multiple deployments are also analyzed. Furthermore, reliability assessment methods are proposed to efficiently solve the reliability.

In this paper, the contributions are summarized as follows: (1) The deployment dynamic model of the folding wing mechanism with joint clearances is established and solved. (2) The reliability models considering failure correlation are established which categorized as with or without

synchronization. (3) Proposing estimation methods for each reliability model, the efficiency and accuracy of the proposed methods are verified by examples. In addition, this paper also studies the reliability variation trend when the random variable distribution parameters are different. It can provide theoretical guidance and data support for the design, manufacture, and work of similar folding wing deployment mechanisms from the perspective of reliability.

The organization of this paper is as follows. Section 2 presents the establishment and solution process of the dynamic model of the folding wing mechanism with joint clearances. Section 3 shows the system reliability model of the folding wing mechanism considering failure correlation, and proposes the corresponding reliability evaluation method to evaluate the system reliability. In Section 4, the correctness of the proposed method is illustrated by the numerical examples, and the system reliability with different random variable parameters is calculated. The conclusion is given in Section 5.

2. Dynamic analysis of folding wing mechanism with joint clearance

2.1. Mechanism composition and transmission principle

In this study, there are four groups of folding wing mechanisms, which are symmetrically arranged in the upper and lower planes of the flight vehicle. There are two groups of folding mechanisms in the upper plane and two groups in the lower plane. As shown in Figure 1, each group of mechanisms contains electric cylinder, main wing, auxiliary wing and slider.

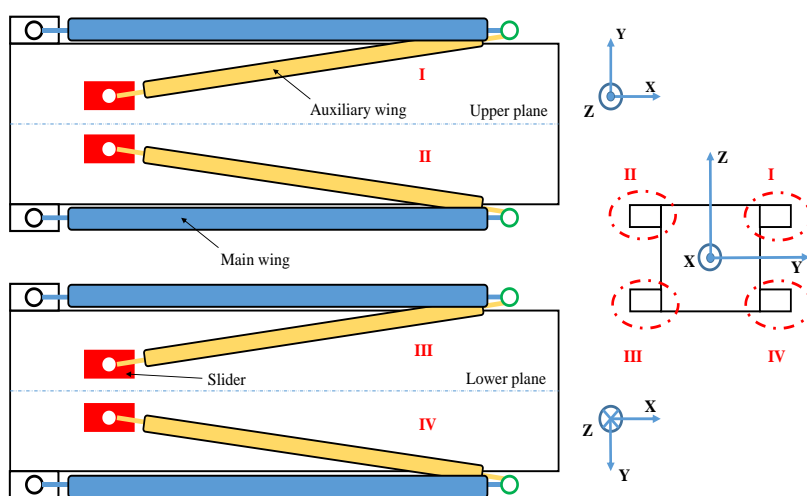


Fig. 1. Structure of folding wing system.

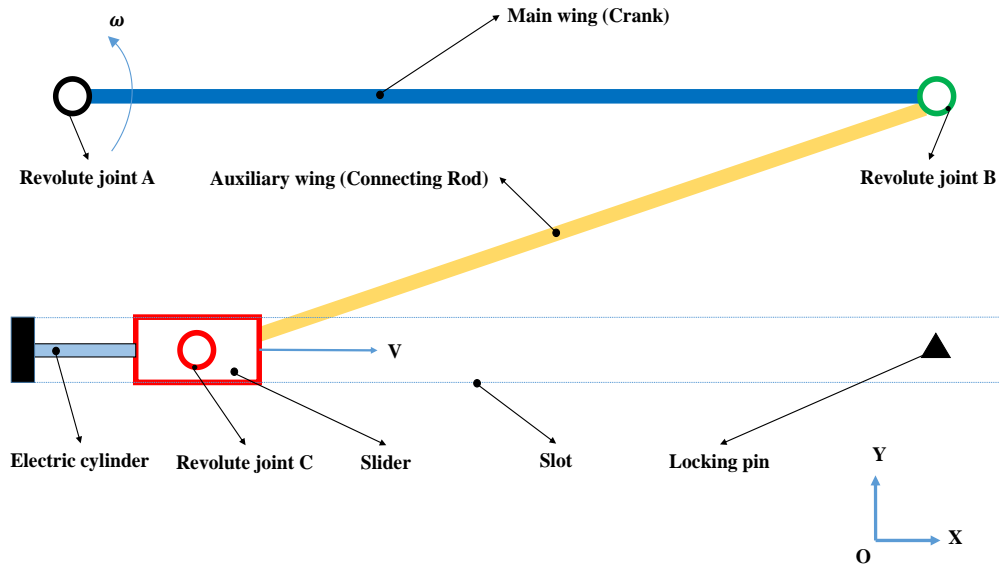


Fig. 2. Folding wing mechanism composition.

The deployment actions of the four groups of folding wing mechanisms are all completed parallel to the XOY plane, the main wing can be simplified as a crank, while the auxiliary wing can be simplified as a connecting rod. As shown in Figure 2, taking the first group of folding wing mechanisms as an example, in the unfolding process, the cylinder will start, the driving force will push the slider to move along the slot, so that the crank will rotate and unfold around the rotation axis A. Finally, the slider reaches the specified locking position, at this time the whole deployment process is finished.

2.2 Contact force analysis of joint with clearance

Generally, the rotating pairs of the mechanism are not ideal. As

shown in Figure 3, the eccentricity vector e is introduced to describe the relative position between the journal and the bearing, which is expressed as 11:

$$e = r_j + A_j s_j^c - r_i - A_i s_i^c \quad (1)$$

where, r_j and r_i are the generalized coordinates of the center of mass for the journal and the bearing components, respectively. A_j and A_i are the transformation matrices of the local coordinate system for the journal and the bearing components with respect to the generalized coordinate system, respectively. s_j^c and s_i^c are the position vectors of the journal center and the bearing center in the local coordinate system, respectively.

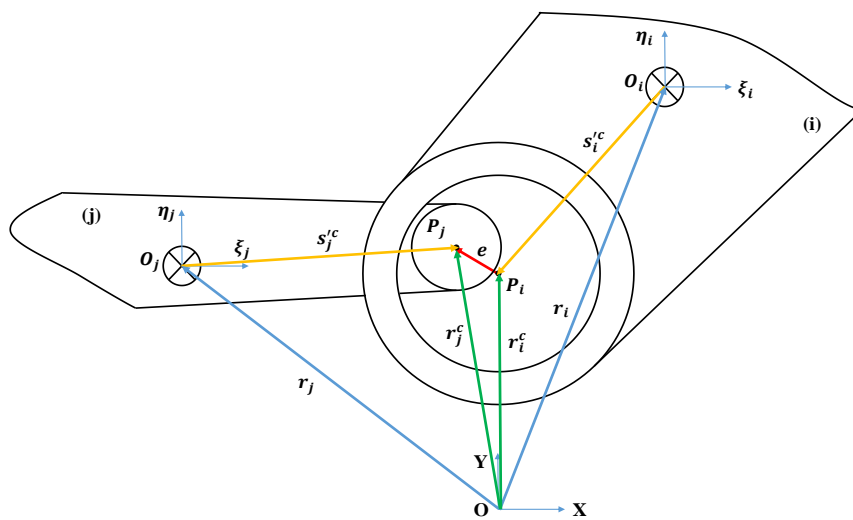


Fig. 3. Relative position of bearing and journal.

When the journal and the bearing collide with each other, as shown in Figure 4, define the unit vector n as the normal vector

at the time of the contact collision.

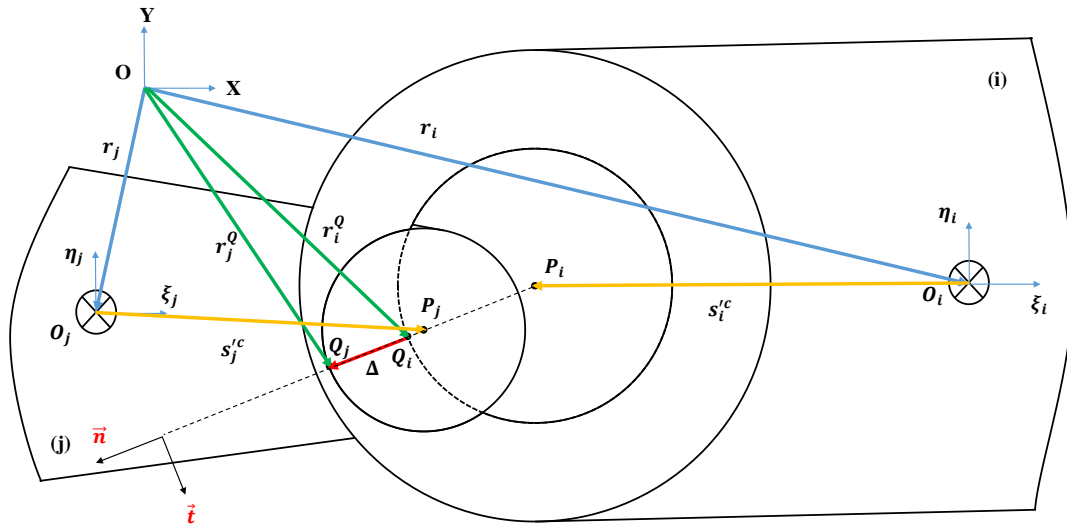


Fig. 4. Collision of bearing and journal.

During the collision phase, there will be a certain penetration depth Δ between the journal and the bearing, which is calculated as:

$$\Delta = (\mathbf{e}^T \mathbf{e})^{1/2} - (R_i - R_j) = (\mathbf{e}^T \mathbf{e})^{1/2} - C_r \quad (2)$$

where, R_i and R_j represent the radii of the bearing and journal, respectively. C_r is the clearance size.

Denoting the contact points between the journal and the bearing during their collision as Q_j and Q_i . The velocity calculation formulas for contact points Q_j and Q_i can be expressed as follows:

$$\begin{cases} \dot{\mathbf{r}}_j^Q = \dot{\mathbf{r}}_j + \dot{\mathbf{A}}_j \mathbf{s}'_j^c + R_j \dot{\mathbf{n}} \\ \dot{\mathbf{r}}_i^Q = \dot{\mathbf{r}}_i + \dot{\mathbf{A}}_i \mathbf{s}'_i^c + R_i \dot{\mathbf{n}} \end{cases} \quad (3)$$

where, the superscripted black dots of the vector represents its first derivative concerning time.

The normal and tangential projections of the relative contact velocity are:

$$\begin{cases} v_n = (\dot{\mathbf{r}}_j^Q - \dot{\mathbf{r}}_i^Q)^T \mathbf{n} \\ v_t = (\dot{\mathbf{r}}_j^Q - \dot{\mathbf{r}}_i^Q)^T \mathbf{t} \end{cases} \quad (4)$$

where, \mathbf{t} represents the unit tangent vector.

The expression for the normal contact force F_N based on the L-N model is given by 10,11,28:

$$F_N = K \Delta^{1.5} \left(1 + \frac{3(1-C_e^2)}{4} \frac{\dot{\delta}}{\dot{\delta}_0} \right) \quad (5)$$

where, C_e represents the restitution coefficient, $\dot{\delta}$ denotes the penetration velocity, $\dot{\delta}_0$ represents the initial penetration velocity. K represents the stiffness coefficient. It can be expressed as:

$$K = \frac{4}{3(h_i + h_j)} \left(\frac{R_i R_j}{R_i + R_j} \right)^{0.5} h_i = \frac{1 - \nu_i^2}{E_i} h_j = \frac{1 - \nu_j^2}{E_j} \quad (6)$$

where, E_i and E_j are the modulus of elasticity of the bearing and journal, respectively. ν_i and ν_j are the Poisson's ratio of the bearing and journal, respectively. R_i and R_j are the radii of the inner circle of the bearing and the outer circle of the journal, respectively.

The calculation equation for the friction force proposed by Ambrósio is given as follows 1:

$$F_T = -c_f c_d F_N \text{sgn}(v_t) \quad (7)$$

where, c_f denotes the friction coefficient, $\text{sgn}(x)$ represents the sign function, and c_d is a dynamic correction parameter that depends on the tangential velocity.

The centroids of the bearing and journal components experience resultant forces:

$$\mathbf{F}_i = F_N \mathbf{n} + F_T \mathbf{t} \mathbf{F}_j = -\mathbf{F}_i \quad (8)$$

The moments experienced at the centroids of the bearing and journal components can be determined as:

$$M_i^c = \mathbf{r}_i^c \times \mathbf{F}_i M_j^c = \mathbf{r}_j^c \times \mathbf{F}_j \quad (9)$$

2.3 Dynamics of folding wing mechanism with joint clearance

As shown in Figure 5, the origin of the generalized coordinates is located at A. The generalized coordinates of the crank, connecting rod, and slider are denoted as (x_1, y_1, θ_1) , (x_2, y_2, θ_2) and (x_3, y_3, θ_3) , respectively. The crank and connecting rod have lengths of l_1 and l_2 . The distance between the slider and the X -axis is denoted as c . Considering the

inclusion of clearances in the rotational pairs B and C. The constraint equations of the folding wing mechanism are as follows:

$$\Phi = \begin{cases} x_1 - \frac{1}{2}l_1 \cos \theta_1 \\ y_1 - \frac{1}{2}l_1 \sin \theta_1 \\ y_3 + c \\ \theta_3 \end{cases} = \mathbf{0} \quad (10)$$

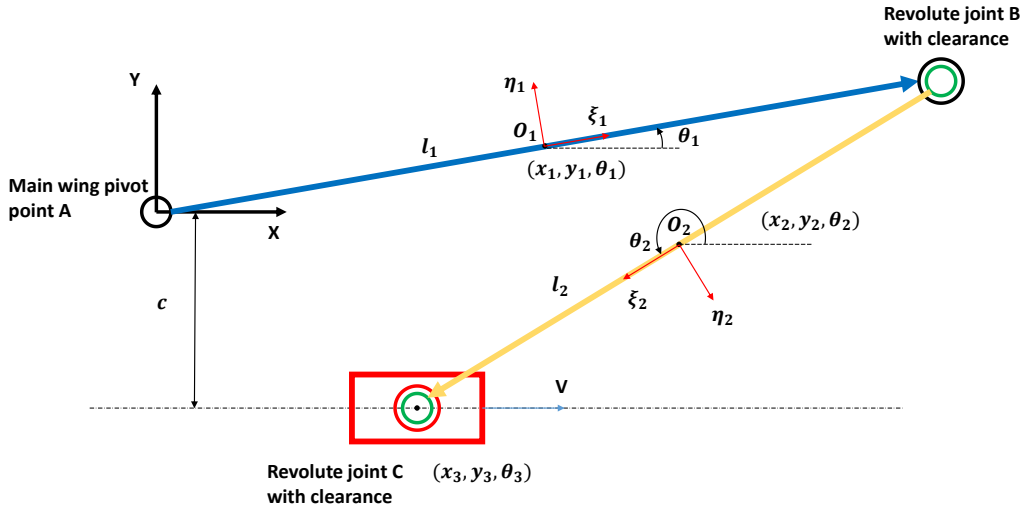


Fig. 5. A set of folding wing mechanism with joint clearances.

According to section 2.2, the contact forces \mathbf{F}_1^Q and \mathbf{F}_2^Q in the joint B, can be determined:

$$\begin{cases} \mathbf{F}_1^Q = F_{1n}\mathbf{n}_1 + F_{1t}\mathbf{t}_1 = [F_{1x}^Q, F_{1y}^Q]^T \\ \mathbf{F}_2^Q = -\mathbf{F}_1^Q = [-F_{1x}^Q, -F_{1y}^Q]^T \end{cases} \quad (11)$$

where, \mathbf{n}_1 and \mathbf{t}_1 are the unit normal and tangent vectors in joint B.

Based on Eq. (8), the expressions for the moments M_1^c and M_2^c at the crank and connecting rod centroids are given by:

$$\begin{cases} M_1^c = \mathbf{r}_{O_1Q_1} \times \mathbf{F}_1^Q \\ M_2^c = \mathbf{r}_{O_2Q_2} \times \mathbf{F}_2^Q \end{cases} \quad (12)$$

where, $\mathbf{r}_{O_1Q_1}$ and $\mathbf{r}_{O_2Q_2}$ are the radius vectors of the crank and connecting rod.

Similarly, the contact forces in the joint C, denoted as \mathbf{F}_3^Q and \mathbf{F}_4^Q , the corresponding moments exerted at the slider and connecting rod are M_3^c and M_4^c .

The folding wing mechanism is also subject to other external forces. The electric cylinder, applies a driving force directly to the center of mass of the slider. The direction always points towards the positive X -axis. The segmental function expression for the variation of the driving force F_d with time t is:

$$F_d = \begin{cases} 100k_d t & 0 \leq t < 0.01 \\ k_d & 0.01 \leq t \leq 0.61 \\ -100k_d t + 62k_d & 0.61 < t \leq 0.62 \end{cases} \quad (13)$$

where, k_d is the peak of the driving force.

During the unfolding process, both the main wing and the auxiliary wing experience aerodynamic loads. The centers of mass of the crank and the connecting rod are subjected to aerodynamic drag forces, denoted as f_1 and f_2 , which act continuously in the positive X -axis direction:

$$f_i = \frac{\rho_a}{2} C_0 b_i |l_i \sin \theta_i| V_q^2 \quad i = 1, 2 \quad (14)$$

where, ρ_a is the air density. C_0 is the air drag coefficient. b_i are the wing thickness. $|l_i \sin \theta_i|$ is the projection length of the folded wing on the Y -axis. V_q is the flight speed of the flight vehicle.

The flight attitude (pitch angle) of the flight vehicle also influences the unfolding dynamics. When the folding wing is not parallel to the ground, the gravitational force can be decomposed into two components along the X -axis and Z -axis directions. The gravitational component along the X -axis will inevitably impact the unfolding behavior. As shown in Figure 6, when the angle between the flight direction and the vertical upward direction of the ground is acute, the pitch angle δ is defined as positive. The magnitude of F_δ can be calculated as:

$$F_\delta^i = |m_i g \sin \delta| \quad i = 1, 2, 3 \quad (15)$$

where, m_i is the mass of the i th component, g is the acceleration of gravity.

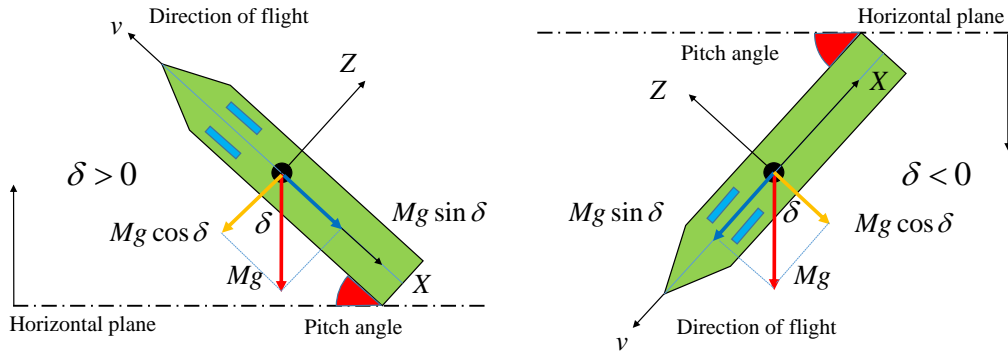


Fig. 6. The flight attitude of flight vehicle.

Figure 7 illustrates the force distribution on the crank, connecting rod and the slider. The generalized force vector \mathbf{Q} can be derived:

$$\mathbf{Q} = \begin{bmatrix} f_1 + m_1 g \sin \delta + F_{1x}^Q \\ F_{1y}^Q \\ M_1^c \\ f_2 + m_2 g \sin \delta - F_{1x}^Q - F_{3x}^Q \\ -F_{1y}^Q - F_{3y}^Q \\ M_2^c + M_4^c \\ m_3 g \sin \delta + F_d + F_{3x}^Q \\ F_{3y}^Q \\ M_3^c \end{bmatrix} \quad (16)$$

The dynamic equations of the folding wing mechanism can be formulated in the index-3 form:

$$\begin{cases} \mathbf{M}\ddot{\mathbf{q}} + \Phi_q^T \lambda = \mathbf{Q} \\ \Phi(\mathbf{q}, t) = \mathbf{0} \end{cases} \quad (17)$$

where, $\ddot{\mathbf{q}}$ represents the second derivative of the generalized coordinates. Φ_q^T denotes the transpose of the Jacobian matrix for constraint equations. λ represents the Lagrange multiplier

vector. \mathbf{M} corresponds to the mass matrix, which can be expressed as:

$$\mathbf{M} = \text{diag}(m_1, m_1, J_1, m_2, m_2, J_2, m_3, m_3, J_3) \quad (18)$$

where, $m_i (i = 1, 2, 3)$ represents the mass of the i th component. $J_i (i = 1, 2, 3)$ represents the moment of inertia for the i th component. These parameters can be further described as:

$$\begin{cases} m_i = \rho_i V_i \\ J_i = \frac{1}{12} m_i (l_i^2 + w_i^2) \end{cases} \quad i = 1, 2, 3 \quad (19)$$

where, ρ_i represents the density of the i th component, while V_i denotes its volume. Additionally, w_i corresponds to the width of the i th component.

The core of the Baumgarte algorithm 2 lies in preventing constraint violation during the numerical solution of Eq. (17).

Based on this, Eq. (17) can be rewritten as:

$$\begin{bmatrix} \mathbf{M} & \Phi_q^T \\ \Phi_q & \mathbf{0} \end{bmatrix} \begin{bmatrix} \ddot{\mathbf{q}} \\ \lambda \end{bmatrix} = \begin{bmatrix} \mathbf{Q} \\ \gamma - 2\alpha(\Phi_q \dot{\mathbf{q}} + \Phi_t) - \beta^2 \Phi \end{bmatrix} \quad (20)$$

where, α and β are stabilization coefficients. $\gamma = \Phi_q \ddot{\mathbf{q}} - (\Phi_q \dot{\mathbf{q}})_q \dot{\mathbf{q}} - 2\Phi_{qt} \dot{\mathbf{q}} - \Phi_{tt}$.

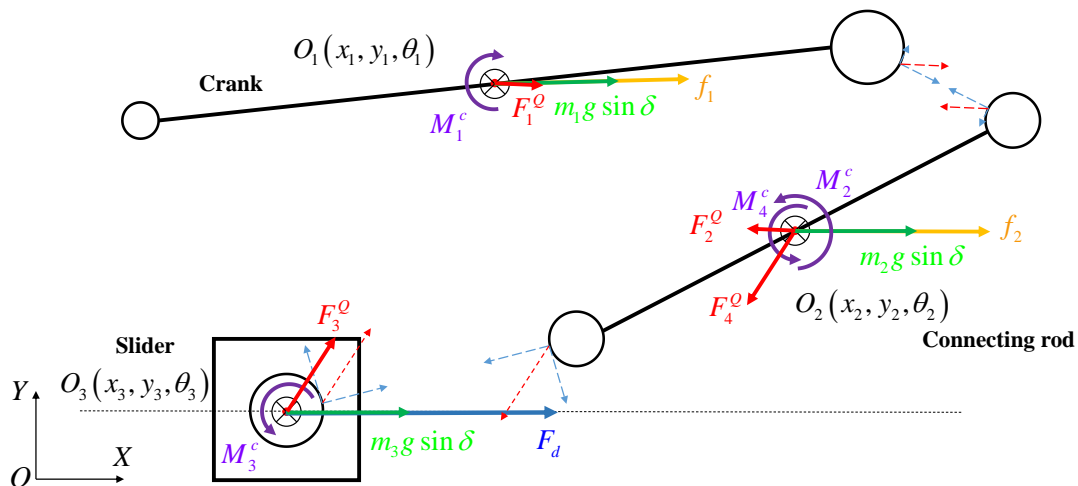


Fig. 7. Force analysis of mechanism components.

The dynamic simulation parameters are shown in Table 1. In this study, we defined the clearance sizes C_r^B and C_r^C in joints B and C as equal. This is because it is possible to reduce the number of random variables in one dimension, which accordingly reduces the samples used for the subsequent reliability analysis and reduces the computational burden. At the same time, such a definition does not materially affect the reliability models and assessment methods proposed in this study. It is the same with b . Based on Eq. (20), a dynamic numerical simulation is conducted, the rotation angle of the main wing is illustrated in Figure 8.

Table 1. Simulation parameters of folded wing mechanism.

Parameters	Value	Parameters	Value
l_1	1500 mm	ρ_a	1.293 kg/m ³
w_1	300 mm	$b_1 = b_2 = b$	7mm
ρ_1	2700 kg/m ³	$C_r^B = C_r^C = C_r$	2.5mm
l_2	1300 mm	R_1^b, R_2^b	10 mm
w_2	200 mm	c	100 mm
ρ_2	2700 kg/m ³	C_e	0.9
V_3	0.001 m ³	E_1	70 GPa
ρ_3	7870 kg/m ³	ν_1	0.33
k_d	550 N	E_2	200 GPa
V_q	140 m/s	ν_2	0.3
δ	0°	C_f	0.1
C_0	1		

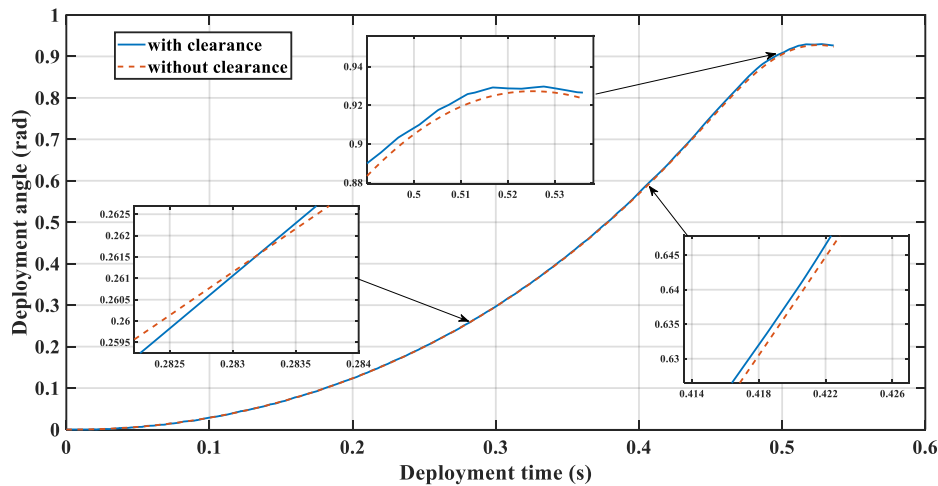


Fig. 8. Main wing rotation angle θ_1 .

3. Reliability analysis of folding wing mechanism system

3.1. System reliability analysis without considering deployment synchronization

3.1.1. Reliability model

Considering the randomness of the operating conditions, actuator performance, design and assembly processes of the folding wing, V_q , δ , b and k_d are treated as normal random variables. Since the sizes of bearings and journals on the folding wing components will have uncertainties in the manufacturing process, which usually obey normal distribution, and since the assembly mode is a clearance fit, there is uncertainty in the clearance size. Through statistical analysis, it can be known that the clearance sizes obey the normal distribution. It is important to note that k_d , b and C_r for each set of folding wing are independent and identically distributed. Defining t_i ($i = 1,2,3,4$) as the actual deployment time for the i th set of folding

wing. We can derive the following expression:

$$t_i = g(V_q, \delta, k_{di}, b_i, C_{ri}) \quad i = 1,2,3,4 \quad (21)$$

where, $g(\bullet)$ represents the deployment time response implicit function. k_{di} , b_i and C_{ri} correspond to the peak of driving force, wing thickness and joint clearance size, respectively, for the i th set of folding wing.

In this study, it is required that t_i for each set of folding wing is less than the threshold T . The deployment performance reliability R_i for any set of folding wing can be expressed as:

$$R_i = Pr\{g(V_q, \delta, k_{di}, b_i, C_{ri}) \leq T\} \quad (22)$$

In practical engineering, the components that make up a system often operate under the same random load environment. Therefore, it is necessary to consider the failure correlation in the system reliability. Based on Eq. (22), it is evident that t_i ($i = 1,2,3,4$) are collectively influenced by V_q and δ . The introduction of V_q and δ results in interdependencies among the failures of the folding wings. When V_q and δ are constant, t_i is

solely determined by k_{di} , b_i and C_{ri} , then the failure events are considered to be mutually independent. The system conditional reliability $R_{S|V_q, \delta}$ can be determined as:

$$R_{S|V_q, \delta} = \prod_{i=1}^4 Pr \{t_{i|V_q, \delta} \leq T\} \quad (23)$$

where, $t_{i|V_q, \delta} = g(k_{di}, b_i, C_{ri}|V_q, \delta)$ is the deployment time of the i th set of folding wing under the condition that V_q and δ are fixed.

Defining $P_{V_q, \delta}^* = Pr \{t_{i|V_q, \delta} \leq T\} (\forall i = 1, 2, 3, 4)$, the probability of all four folding wing mechanisms in the system operating normally under random V_q and δ is the mathematical expectation of their conditional reliability function:

$$\begin{aligned} R_s &= \int_{V_q, \delta} f_{V_q}(V_q) f_{\delta}(\delta) \left[\prod_{i=1}^4 Pr \{t_{i|V_q, \delta} \leq T\} \right] d\delta dV_q \\ &= \int_{V_q, \delta} f_{V_q}(V_q) f_{\delta}(\delta) [P_{V_q, \delta}^*]^4 d\delta dV_q \end{aligned} \quad (24)$$

where, $f_{V_q}(V_q)$ and $f_{\delta}(\delta)$ are the probability density functions of V_q and δ .

Furthermore, after each flight mission, every set of folding wing mechanism needs to be disassembled and replaced. The conditional PDF of $t_{i|V_q, \delta}$ can be defined as $h_{t_{i|V_q, \delta}}(t_i|V_q, \delta)$. Then Eq. (24) can be rewritten as:

$$R_s = \int_{V_q, \delta} f_{V_q}(V_q) f_{\delta}(\delta) \left[\prod_{i=1}^4 \int_0^T h_{t_{i|V_q, \delta}}(t_i|V_q, \delta) dt_i \right] d\delta dV_q \quad (25)$$

When a flight vehicle operates under a specified airspace, its flight velocity V_q and flight attitude (pitch angle δ) are constant. However, there are many airspaces in which the vehicle operates, which are defined here as Ω_j , ($j = 1, 2, \dots, n_a$). Statistical analysis of the obtained data shows that V_q and δ of the flight vehicle in these airspaces follow the normal distribution. In this study, according to the task description and regulations given in the engineering project, the flight vehicle will complete multiple missions, not only that, in multiple missions, the flight vehicle needs to continue to work in the same airspace, which means that in the process of completing multiple missions, the folding wing mechanisms on the flight vehicle will be deployed in the same airspace. However, during the first mission, the airspace in which the flight vehicle is operating is random, and therefore V_q and δ of the vehicle are random during the first mission. Upon completion of the first mission, the airspace in which the vehicle operates can be determined, which in turn allows for the determination of V_q and

δ under subsequent missions. That is, V_q and δ during the first mission are the observation values under the respective distributions, while V_q and δ during the subsequent missions are equal to the observation values. Let $t_{i|V_q, \delta}^j$, $j = 1, 2, \dots, m$ be defined as the deployment time of the i th set of folding wing under the fixed V_q and δ during the j th deployment event. By arranging $t_{i|V_q, \delta}^j$ in ascending order, we obtain the order statistics $t_{i|V_q, \delta}^{(1)}, t_{i|V_q, \delta}^{(2)}, \dots, t_{i|V_q, \delta}^{(m)}$. The probability density function of $t_{i|V_q, \delta}^{(m)}$ is:

$$h_{t_{i|V_q, \delta}^{(m)}}(t_i|V_q, \delta) = m [H_{t_{i|V_q, \delta}}(t_i|V_q, \delta)]^{m-1} h_{t_{i|V_q, \delta}}(t_i|V_q, \delta) \quad (26)$$

where, $H_{t_{i|V_q, \delta}}(t_i|V_q, \delta)$ represents the conditional cumulative distribution function (CDF) of $t_{i|V_q, \delta}$.

When V_q and δ are fixed, the probability that the i th set of folding wing successfully unfolds in all m flight missions can be expressed as:

$$Pr \{ \bigcap_{j=1}^m t_{i|V_q, \delta}^j \leq T \} = Pr \{ t_{i|V_q, \delta}^{(m)} \leq T \} \quad (27)$$

The system deployment performance reliability after m flight missions is:

$$R_s^m = \int_{V_q, \delta} f_{V_q}(V_q) f_{\delta}(\delta) [H_{t_{i|V_q, \delta}}(T|V_q, \delta)]^{4m} d\delta dV_q \quad (28)$$

Considering the uncertainty associated with the actual number of completed missions m during the designated operational period, it is typical to establish a predetermined total number of flight missions N_t to be accomplished. The probability of successfully completing each individual mission is denoted by p_m , and the outcomes of mission completion are mutually independent. Consequently, the actual number of completed missions m in N_t planned flights follows a binomial distribution, which can be expressed as follows:

$$Pr \{ m = k \} = C_{N_t}^k p_m^k (1 - p_m)^{N_t - k} \quad k = 0, 1, 2, \dots, N_t \quad (29)$$

Based on Eq. (28)-(29), the expression for the system deployment performance reliability, without considering synchronization, can be obtained using the law of total probability:

$$R_s = \sum_{k=0}^{N_t} C_{N_t}^k p_m^k (1 - p_m)^{N_t - k} \cdot \int_{V_q, \delta} f_{V_q}(V_q) f_{\delta}(\delta) [H_{t_{i|V_q, \delta}}(T|V_q, \delta)]^{4k} d\delta dV_q \quad (30)$$

3.1.2. Reliability assessment method

The efficiency of MCS is hindered by the integration operations and unknown conditional cumulative distribution functions. The surrogate models demand numerous samples for precise global models, they also spend much time in predicting small failure probabilities through large training sets. Numerical integration methods strike a balance between efficiency and accuracy for integration tasks. Additionally, SPA excels in estimating distribution function tails. Thus, this study employs the numerical integration and SPA to solve the reliability issues.

The Gauss-Hermite quadrature formula is utilized to handle the integration operation in Eq. (30), and the full factorial numerical integration (FFNI) method is applied to discretize the integration operation in Eq. (30), resulting in:

$$R_s = \sum_{k=0}^{N_t} C_{N_t}^k p_m^k (1 - p_m)^{N_t-k} \cdot \left[\frac{1}{\pi} \sum_{q_1=1}^{m_1} \sum_{q_2=1}^{m_2} w_{q_1} w_{q_2} H_{t_i|V_{q_1}, \delta}^{4k} \left(T \sqrt{2} \sigma_{V_{q_1}} \alpha_{q_1} + \mu_{V_{q_1}} \sqrt{2} \sigma_{\delta} \alpha_{q_2} + \mu_{\delta} \right) \right] \quad (31)$$

where, m_1 and m_2 represent the number of integration nodes. w_{q_1} and w_{q_2} denote the integration weights. α_{q_1} and α_{q_2} represent the integration nodes. $\mu_{V_{q_1}}$ and μ_{δ} are the means. $\sigma_{V_{q_1}}$ and σ_{δ} are the standard deviations.

For $H_{t_i|V_{q_1}, \delta}$, it can be solved using SPA. Let $Y = g(\mathbf{X})$, an approximate method 16,46 can be used to estimate the cumulant-generating function (CGF) of Y , given by the

following expression:

$$\tilde{K}_Y(t) = \kappa_1 t + \kappa_2 \frac{t^2}{2} + \kappa_3 \frac{t^3}{6} + \kappa_4 \frac{t^4}{24} \quad (32)$$

where, $\kappa_i (i = 1, 2, 3, 4)$ is the i th cumulant of Y :

$$\begin{cases} \kappa_1 = \mu'_1 \\ \kappa_2 = \mu'_2 - \mu'^2_1 \\ \kappa_3 = \mu'_3 - 3\mu'_2\mu'_1 + 2\mu'^3_1 \\ \kappa_4 = \mu'_4 - 4\mu'_3\mu'_1 - 3\mu'^2_2 + 12\mu'_2\mu'^2_1 - 6\mu'^4_1 \end{cases} \quad (33)$$

where, $\mu'_i (i = 1, 2, 3, 4)$ are the first four raw moments of Y .

The real number saddle point s_r at $Y = y$ can be determined:

$$\kappa_1 + \kappa_2 s_r + \kappa_3 \frac{s_r^2}{2} + \kappa_4 \frac{s_r^3}{6} - y = 0 \quad (34)$$

The expression of the CDF for Y is 6:

$$F_Y(y) = \Phi(w) + \varphi(w) \left(\frac{1}{w} - \frac{1}{v} \right) \quad (35)$$

where, $\Phi(*)$ and $\varphi(*)$ are the CDF and PDF of the standard normal variable. The parameters w and v are:

$$\begin{cases} w = \text{sgn}(s_r) \sqrt{2[s_r y - \tilde{K}_Y(s_r)]} \\ v = s_r \sqrt{\ddot{\tilde{K}}_Y(s_r)} \end{cases} \quad (36)$$

where, $\ddot{\tilde{K}}_Y(s_r)$ is the second derivative of the CGF for Y at s_r .

To compute $\mu'_i (i = 1, 2, 3, 4)$, the use of the FFNI method and Gauss quadrature formula is necessary. Once the conditional CDFs for all nodes are obtained, the system reliability without synchronization can be calculated. The specific process is illustrated in Figure 9.

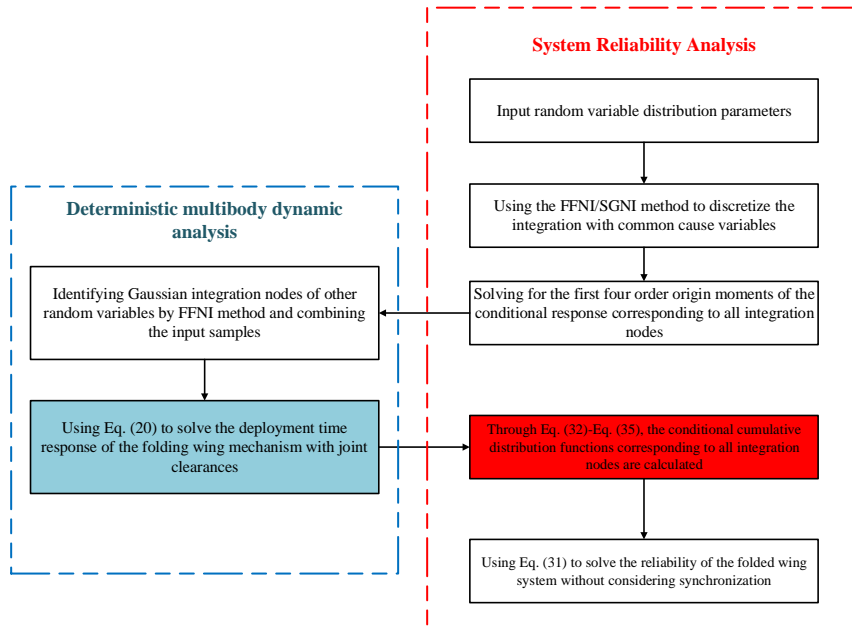


Fig. 9. Reliability assessment process without synchronization.

3.2. System reliability analysis considering deployment synchronization

3.2.1. Reliability model

In some extreme conditions, the deployment time of each folding wing should not differ too much. Otherwise, it will result in a reduction of stability. In this case, the deployment synchronization reliability also needs to be considered. In this study, the difference between the maximum and minimum deployment time within the system is taken as the indicator. The system reliability R_s^* considering synchronization for one flight mission can be expressed as:

$$R_s^* = \int_{V_q, \delta} f_{V_q}(V_q) f_{\delta}(\delta) \left[Pr \left\{ \max t_{i|V_q, \delta} \leq T, \max t_{i|V_q, \delta} - \min t_{i|V_q, \delta} \leq \tau \right\} \right] d\delta dV_q \quad (37)$$

where, τ is the given difference value threshold. Let $\varepsilon_{t|V_q, \delta} = \max t_{i|V_q, \delta} - \min t_{i|V_q, \delta}$, $\xi_{t|V_q, \delta} = \max t_{i|V_q, \delta}$. When V_q and δ are fixed, the conditional reliability $R_{s|V_q, \delta}^m$ of the folding wing system for m flight missions can be expressed as follows:

$$R_{s|V_q, \delta}^m = Pr \left\{ \bigcap_{i=1}^m \xi_{t|V_q, \delta}^{(i)} \leq T, \bigcap_{i=1}^m \varepsilon_{t|V_q, \delta}^{(i)} \leq \tau \right\} \quad (38)$$

where, the symbol (i) in the upper right corner represents the i th flight mission.

By combining Eq. (37) and Eq. (38), the reliability R_s^{*m} of the folding wing system for m flight missions can be obtained as follows:

$$R_s^{*m} = \int_{V_q, \delta} f_{V_q}(V_q) f_{\delta}(\delta) R_{s|V_q, \delta}^{*m} d\delta dV_q \quad (39)$$

The total reliability of the folding wing system considering synchronization is:

$$R_s^* = \sum_{k=0}^{N_t} C_{N_t}^k p_m^k (1 - p_m)^{N_t - k} \cdot R_s^{*k} \quad (40)$$

3.2.2. Reliability assessment method

When calculating $\varepsilon_{t|V_q, \delta}$ and $\xi_{t|V_q, \delta}$, $t_{i|V_q, \delta}$ ($i = 1, 2, 3, 4$) need to be calculated, so the reliability model that introduces synchronization is more complex and difficult to solve. Due to the long computational time required for solving the multibody dynamic with clearances, MCS is difficult to accept. Using large training datasets for surrogate models can significantly extend computational time, especially when predicting responses for multiple flight missions. Therefore, this section presents an efficient approach combining Gaussian integration with the Pearson distribution family to solve the reliability model.

Additionally, numerical simulation techniques are also applied.

The Pearson distribution family allows the representation of the distribution's parameters as functions of the first four moments. Let $Z = g(\mathbf{X})$ be the performance function, then the mean μ_Z , standard deviation σ_Z , skewness α_{3g} and kurtosis α_{4g} of Z are:

$$\begin{cases} \mu_Z = \int Z f(\mathbf{X}) d\mathbf{X} \\ \sigma_Z = \sqrt{\int (Z - \mu_Z)^2 f(\mathbf{X}) d\mathbf{X}} \\ \alpha_{3g} = \int \left(\frac{Z - \mu_Z}{\sigma_Z} \right)^3 f(\mathbf{X}) d\mathbf{X} \\ \alpha_{4g} = \int \left(\frac{Z - \mu_Z}{\sigma_Z} \right)^4 f(\mathbf{X}) d\mathbf{X} \end{cases} \quad (41)$$

The PDF f of the standardized variable Z_u satisfies the given differential equation 40,41,42:

$$\frac{1}{f} \frac{df}{dZ_u} = -\frac{aZ_u + b}{c + bZ_u + dZ_u^2} \quad (42)$$

where, $Z_u = \frac{Z - \mu_Z}{\sigma_Z}$. The coefficients a , b , c and d are related to the first four moments.

It is now illustrated with a folding wing system, μ_Z , σ_Z , α_{3g} and α_{4g} of $t_{i|V_q, \delta}$ can be solved by the FFNI method, then a , b , c and d can be calculated. Subsequently, $\hat{h}_{i|V_q, \delta}(t_i|V_q, \delta)$ will be approximated. It is important to note that we need to solve for both the maximum and minimum values of $t_{i|V_q, \delta}$. Fortunately, methods such as inverse transform sampling can be employed to generate sufficient samples from $\hat{h}_{i|V_q, \delta}(t_i|V_q, \delta)$, $i = 1, 2, 3, 4$. Assuming that a total of N_0 samples are generated, then $N_0 \times 4$ observations with $t_{i|V_q, \delta}$ ($i = 1, 2, 3, 4$) can be obtained:

$$\mathbf{t} = \begin{bmatrix} t_{11} & t_{12} & t_{13} & t_{14} \\ t_{21} & t_{22} & t_{23} & t_{24} \\ \vdots & \vdots & \vdots & \vdots \\ t_{N_0 1} & t_{N_0 2} & t_{N_0 3} & t_{N_0 4} \end{bmatrix} \quad (43)$$

where, the second number in the lower right corner represents the number of groups.

The conditional system reliability with a single flight mission:

$$R_{s|V_q, \delta}^* = \frac{1}{N_0} \sum_{l=1}^{N_0} I(\mathbf{t}_l^{row}) \quad (44)$$

where, \mathbf{t}_l^{row} represents the l th row in the matrix \mathbf{t} , $\mathbf{t}_l^{row} = [t_{l1}, t_{l2}, t_{l3}, t_{l4}]$. $I(\mathbf{t}_l^{row})$ denotes the indicator function, which can be expressed as follows:

$$I(\mathbf{t}_l^{row}) = \begin{cases} 1 & \max \mathbf{t}_l^{row} - \min \mathbf{t}_l^{row} \leq \tau \cap \max \mathbf{t}_l^{row} \leq T \\ 0 & \text{otherwise} \end{cases} \quad (45)$$

When the flight vehicle performs m missions, it is repeated

m times to generate the sample set of $t_{i|V_q,\delta}$. The sample set is defined as:

$$\mathbf{t}_m = \begin{bmatrix} t_{11}^{(1)} & t_{12}^{(1)} & t_{13}^{(1)} & t_{14}^{(1)} & \cdots & t_{11}^{(m)} & t_{12}^{(m)} & t_{13}^{(m)} & t_{14}^{(m)} \\ t_{21}^{(1)} & t_{22}^{(1)} & t_{23}^{(1)} & t_{24}^{(1)} & \cdots & t_{21}^{(m)} & t_{22}^{(m)} & t_{23}^{(m)} & t_{24}^{(m)} \\ \vdots & \vdots \\ t_{N_01}^{(1)} & t_{N_02}^{(1)} & t_{N_03}^{(1)} & t_{N_04}^{(1)} & \cdots & t_{N_01}^{(m)} & t_{N_02}^{(m)} & t_{N_03}^{(m)} & t_{N_04}^{(m)} \end{bmatrix}_{N_0 \times 4m} \quad (46)$$

where, the upper right corner symbol represents the number of times the mission was performed.

The conditional reliability with synchronization, after performing m flight missions, can be calculated:

$$R_{s|V_q,\delta}^{*(m)} = \frac{1}{N_0} \sum_{l=1}^{N_0} [\prod_{k=1}^m I(\mathbf{t}_l^{(k)row})] \quad (47)$$

where, $\mathbf{t}_l^{(k)row} = [t_{l1}^{(k)}, t_{l2}^{(k)}, t_{l3}^{(k)}, t_{l4}^{(k)}]$.

By combining Eq. (47) with Eq. (39)-(40), the total reliability, denoted as R_s^* , can be efficiently computed. The entire calculation process is illustrated in Figure 10.

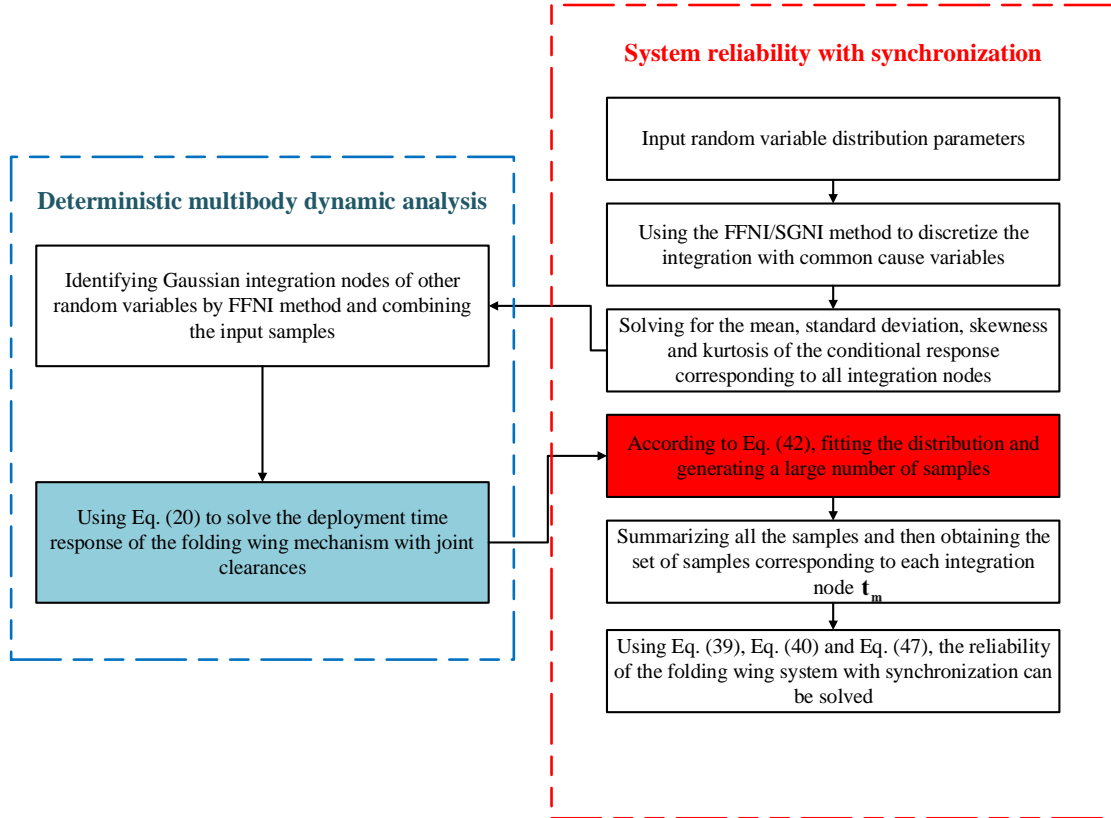


Fig. 10. Reliability assessment process with synchronization.

4. Examples of reliability analysis

In this section, the first three examples are used to validate the accuracy of the proposed method by MCS. It should be noted that obtaining high-precision dynamic responses requires a significant amount of simulation time. Consequently, using MCS to compute the reliability in the fourth and fifth examples is not practical. Furthermore, the purpose of the fourth and fifth examples is to explore the variation trends of the system reliability under different random variable conditions. The sixth example is to explore the variation law of the reliability considering the randomness of the folding wing lengths. So only the proposed method is used in the fourth, fifth and sixth

examples.

4.1. Mathematical example

Consider a series system containing four units as shown in Figure 11. The response of each unit is:

$$\begin{aligned} Y_1 &= \exp(0.1X_1 + 0.2) - \exp(0.2X_2 + X_3) - 4(X_1 + 1.5X_2 - 1)^3 + 18 \\ Y_2 &= \exp(0.1X_1 + 0.2) - \exp(0.2X_4 + X_5) - 4(X_1 + 1.5X_4 - 1)^3 + 18 \\ Y_3 &= \exp(0.1X_1 + 0.2) - \exp(0.2X_6 + X_7) - 4(X_1 + 1.5X_6 - 1)^3 + 18 \\ Y_4 &= \exp(0.1X_1 + 0.2) - \exp(0.2X_8 + X_9) - 4(X_1 + 1.5X_8 - 1)^3 + 18 \end{aligned} \quad (48)$$

The series system of example 1

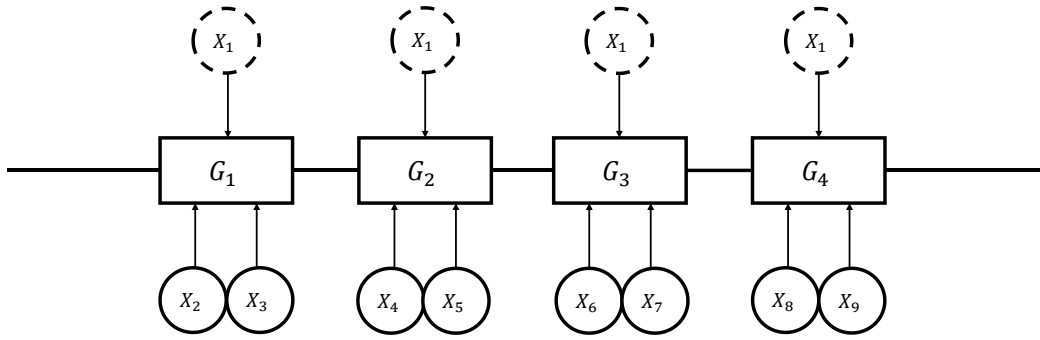


Fig. 11. Illustration of the system in Example 1.

The random variables are mutually independent, and the distribution parameters are shown in Table 2.

Table 2. Random variables and distributed parameters in example 1.

Random variables	Distribution	Mean value	Standard deviation
X_1	Normal	1	0.05
X_2, X_4, X_6, X_8	Normal	1.2	0.05
X_3, X_5, X_7, X_9	Normal	0.5	0.1

Defining the response threshold as T_1 . The system reliability at one working time is shown in Figure 12(a). When the system works m times, the system works for the k th ($k \geq 2$) time and the observations of X_1 are the same as for the first time. The calculated results of system reliability are shown in Figure 12(b). As m increases, the dispersion of the system response $\bigcap_{k=1}^m \max_{1 \leq i \leq 4} Y_i^{(k)}$ decreases. The difference $\max_{1 \leq i \leq 4} Y_i - \min_{1 \leq i \leq 4} Y_i$ needs to be less than the given threshold τ_1 . Figure 12(c) presents the reliability curves for $m = 2$ and $m = 5$, as τ_1 increases, the system reliability also increases. For any given operating condition, the reliability increase rate gradually diminishes until it reaches a nearly constant level.

The sample sizes for both methods are listed in Table 3. The relative errors compared to the MCS are listed in Figure 12(d)-12(e). In this study, the calculation error of the proposed method is determined by the relative error of the failure probability, the expression is:

$$err = \frac{|R_p - R_{MCS}|}{1 - R_{MCS}} \quad (49)$$

where, R_p is the reliability obtained by the proposed method. R_{MCS} is the reliability obtained by MCS. In fact, all the calculation results based on MCS and the proposed method are approximate consistent. At the same time, the number of samples required by the proposed method is also small.

Table 3. The sample sizes for both methods in Example 1.

Methods	Sample size(without synchronization)	Sample size(with synchronization)
MCS	2×10^6	2×10^6
The proposed method	75	75

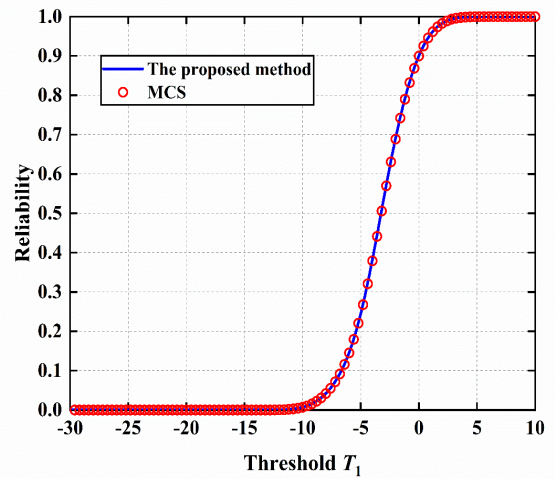


Fig. 12. (a) Reliability curve without synchronization for $m=1$.

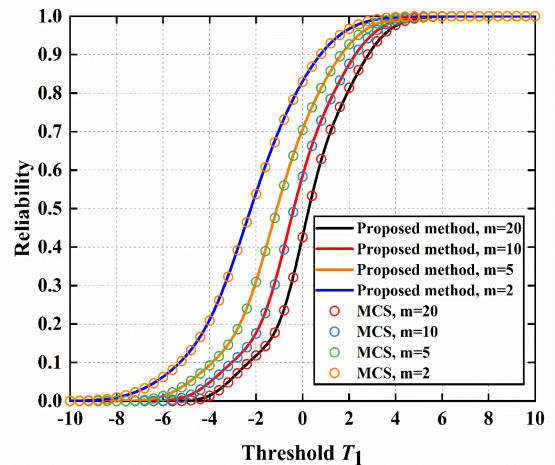


Fig. 12.(b) Reliability curves without synchronization for $m>1$.

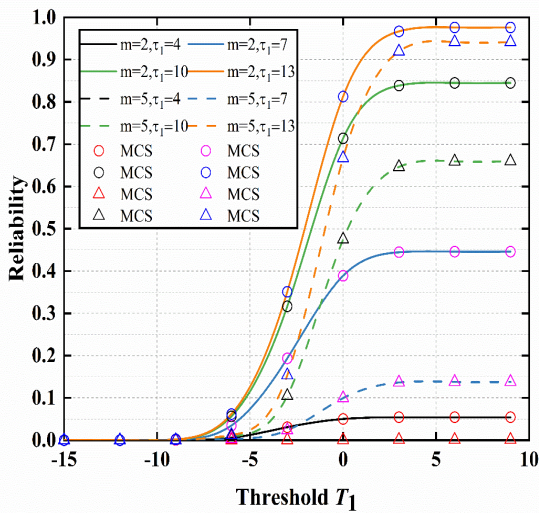


Fig. 12.(c) Reliability curves with synchronization for $m > 1$.

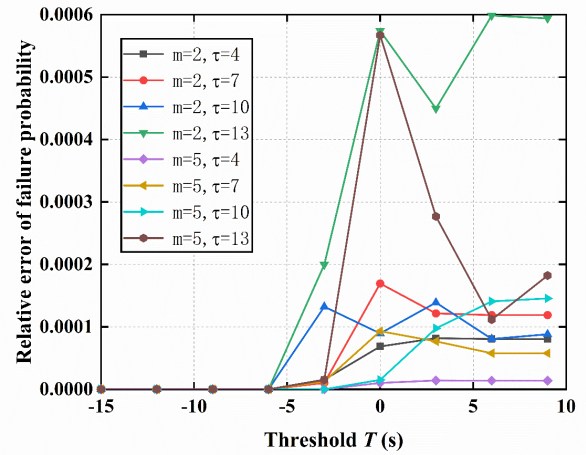


Fig. 12.(e) Failure probability relative error with synchronization for Example 1.

4.2. Motion reliability of the four-bar mechanism system

Consider a four-bar mechanism system as shown in Figure 13. The system consists of two sets of four-bar mechanisms, with the driving link rod 1 being shared by both sets. The length of each rod is denoted by $R_i (i = 1, 2, \dots, 7)$. The rod length distribution parameters are in Table 4.

Table 4. Distribution parameters for each rod length.

Random variables	Distribution	Mean value (mm)	Standard deviation (mm)
R_1	Normal	53	1
R_2, R_4, R_6	Normal	122	1
R_3, R_5, R_7	Normal	66.5	1

Taking the first group of four-bar mechanism as an example, output angle φ_3 is:

$$\varphi_3 = 2 \arctan \frac{D \pm \sqrt{D^2 + E^2 - F^2}}{E + F} \quad (50)$$

where, $D = -2R_1R_3 \sin \theta$, $E = 2R_3(R_4 - R_1 \cos \theta)$, $F = R_2^2 - R_1^2 - R_3^2 - R_4^2 + 2R_1R_4 \cos \theta$. The value of θ in this example is 100.5° .

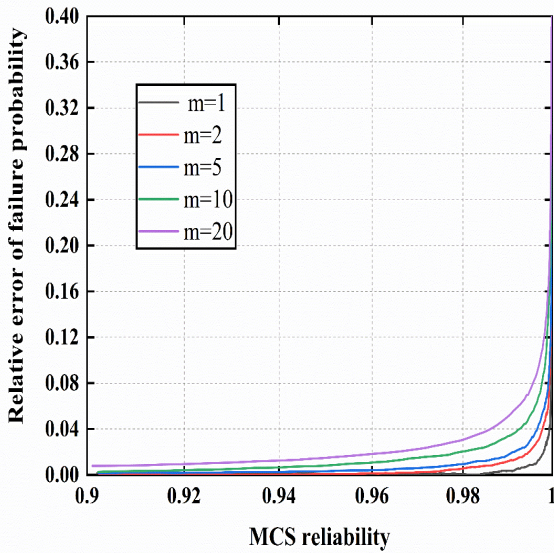


Fig. 12.(d) Failure probability relative error without synchronization for Example 1.

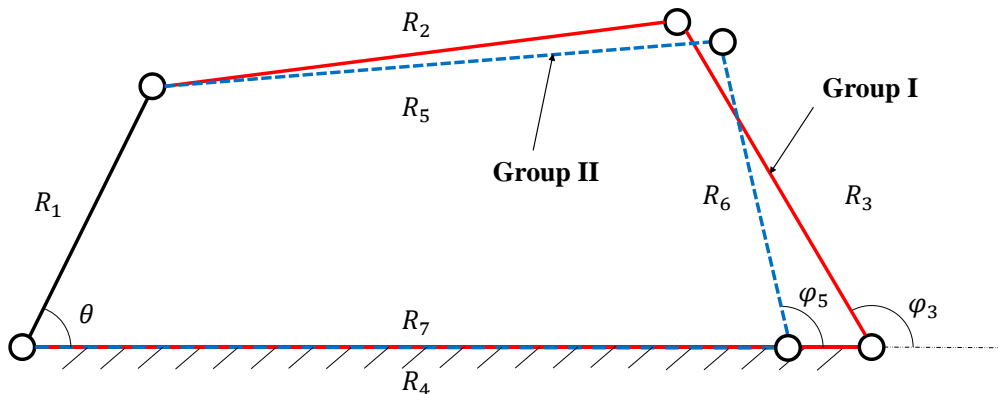


Fig. 13. Two sets of four-bar mechanisms.

It is defined that the system is failure when φ_3 and φ_5 exceed the threshold T_2 . The reliability is illustrated in Figure 14(a). Consider this system that operates for a total of m times, and at the k th ($k \geq 2$) operation, each rod, except rod 1, is removed and replaced. Then the positioning reliability is shown in Figure 14(b). As m increases, the reliability and the system response dispersion become smaller. Introducing $\max_{i=3,5} \varphi_i - \min_{i=3,5} \varphi_i$ to describe the difference in output angles. The synchronization threshold is τ_2 . The system reliability curves for $m = 2$ and $m = 5$ are given in Figure 14(c). A higher value of τ_2 leads to higher reliability. With the continuous increase of T_2 , the increment of reliability becomes smaller until it reaches a plateau. The MCS results also confirm the accuracy of the proposed method in all cases. The sample sizes for both methods are listed in Table 5. The relative errors compared to the MCS are listed in Figure 14(d)-14(e).

Table 5. The sample sizes for both methods in Example 2.

Methods	Sample size(without synchronization)	Sample size(with synchronization)
MCS	3×10^6	3×10^6
The proposed method	375	375

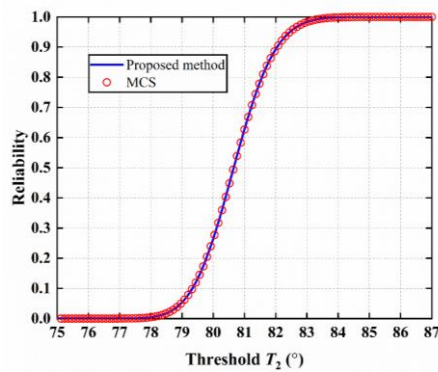


Fig. 14(a). Reliability curve without synchronization for $m=1$.

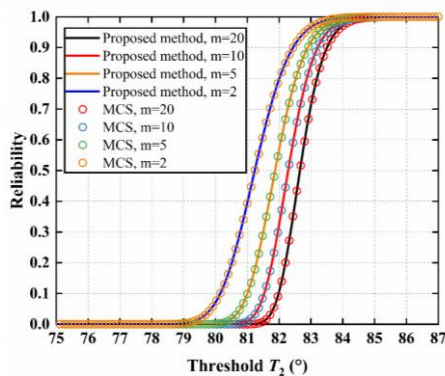


Fig. 14(b). Reliability curves without synchronization for $m > 1$.

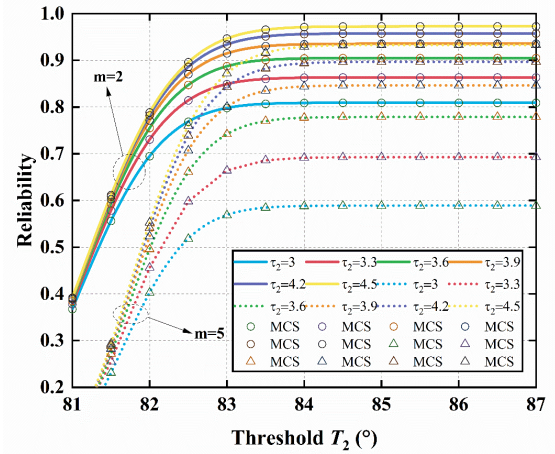


Fig. 14(c). Reliability curves with synchronization for $m > 1$.

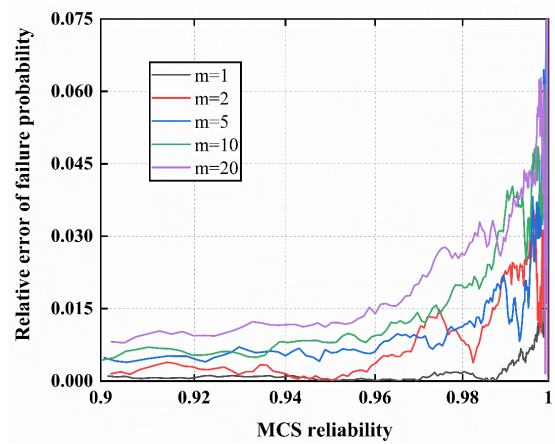


Fig. 14(d). Failure probability relative error without synchronization for Example 2.

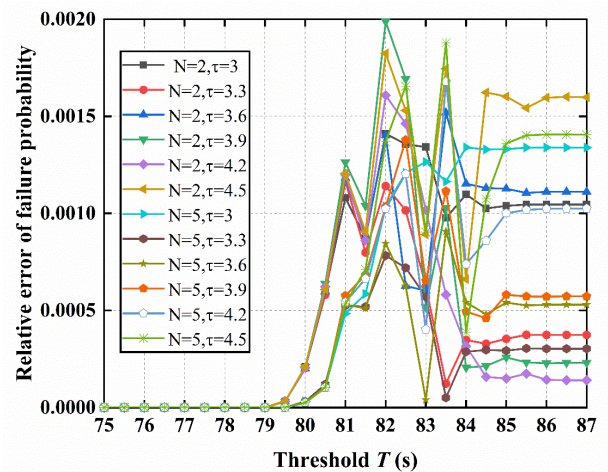


Fig. 14(e). Failure probability relative error with synchronization for Example 2.

4.3. Deployment performance reliability of folding wing system

The random variables of the folding wing mechanism system are shown in Table 6.

Table 6 Distribution parameters of random variables for folding wing system

Parameter	Unit	Distribution	Mean value	Standard deviation
V_q	m/s	Normal	140	10
δ	°	Normal	0	5
$k_{d1}, k_{d2}, k_{d3}, k_{d4}$	N	Normal	550	10
b_1, b_2, b_3, b_4	mm	Normal	7	0.25
$C_{r1}, C_{r2}, C_{r3}, C_{r4}$	mm	Normal	1.5	0.05

Figure 15(a) depicts the reliability under m ($m = 2, 5, 8, 10$) flight missions. As m increases, the reliability and system response dispersion decreases. The case where synchronization is included is shown in Figure 15(b). When T is greater than 0.57 s, the size of τ becomes the main factor influencing reliability. When T is less than 0.545 s, the size of T becomes the main factor. Figure 15(c) presents the reliability for different values of m , τ , and T . When T is greater than 0.57 s, the larger the value of τ is, the denser the reliability curves corresponding to different times m are. Considering the uncertainty of m , as shown in Figure 15(d), p_m is 0.5 and the expected number of planned flights is N_t ($N_t = 2, 4, 6, 8, 10$). For the given τ and T ($T \in [0.545, 0.57]$), the reliability increases with decreasing N_t . When T exceeds 0.57 s, a higher value of τ results in denser reliability curves corresponding to different N_t . Figure 15(e) illustrates the reliability under different p_m , with N_t set to 10. Under the given τ and T , the system reliability decreases with an increase in p_m . When T exceeds 0.57 s, higher values of τ result in denser reliability curves corresponding to different p_m . It is evident that both the deployment time threshold T and the number of deployment times m significantly influence the system reliability. In the context of considering the deployment synchronization, at any given T and τ level, an increase in m leads to lower system reliability. At any given T and m level, an increase in τ leads to higher system reliability. As T increases, the system reliability first gradually increases and then reaches a stable state. Taking into consideration the uncertainty of m , under the given T , τ and p_m , a smaller N_t leads to higher system reliability. Under the given T , τ and N_t , a higher p_m results in lower system reliability.

The sample sizes for both methods are listed in Table 7. The relative errors compared to the MCS are listed in Figure 15(f)-15(g). According to the MCS results, the proposed methods are suitable for solving the reliability of the folding wing system.

In order to visualize the differences between the failure

independent case and failure correlation case, the differences are shown in Figure 15(h). As can be seen from the figure, in the folding wing series system, the results in the assumed independent case are more conservative compared to the case where failure correlation is considered. Also, the difference between the two cases becomes smaller as the threshold increases. However, when the threshold is a constant value, the difference gradually increases as the number of components n in the system increases, and the results obtained based on the assumed independent case become less accurate.

Table 7. The sample sizes for both methods in Example 3.

Methods	Sample size (without synchronization)	Sample size (with synchronization)
MCS	2×10^6	1.2×10^6
The proposed method	1125	1125

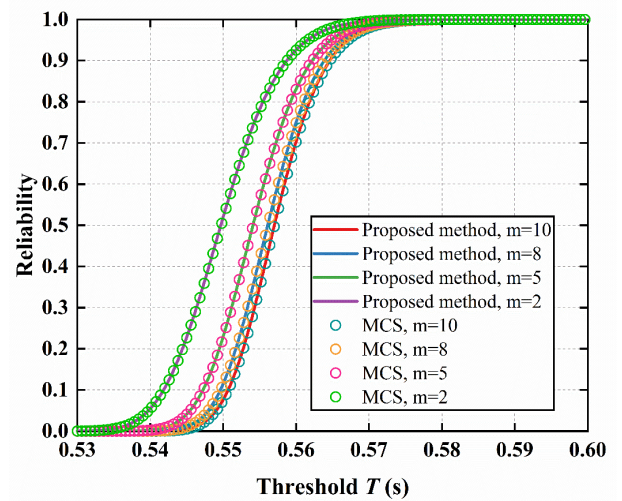


Fig. 15(a). Reliability curves without synchronization for $m > 1$.

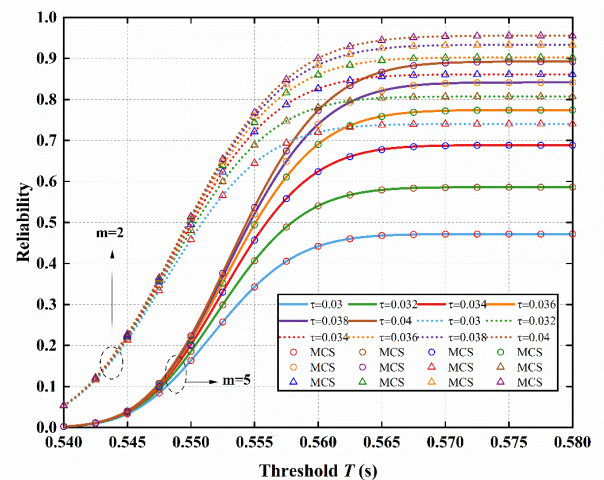


Fig. 15(b). Reliability curves with synchronization for $m > 1$.

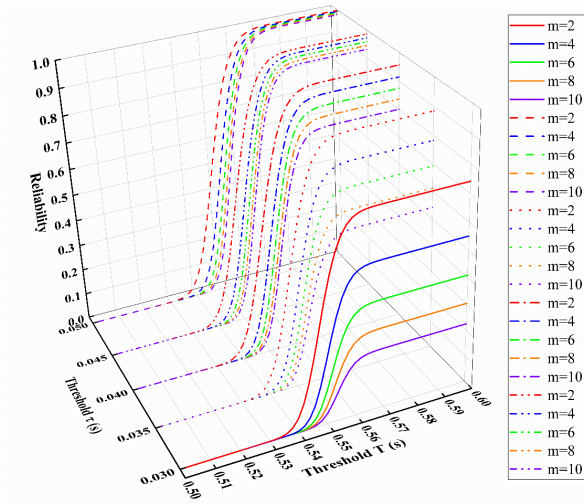


Fig. 15(c). Reliability curves for different values of m , τ and T

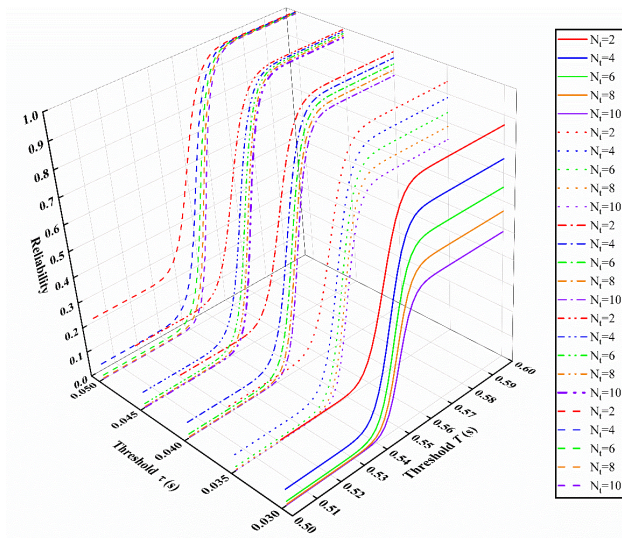


Fig. 15(d). Reliability curves with synchronization for different N_t

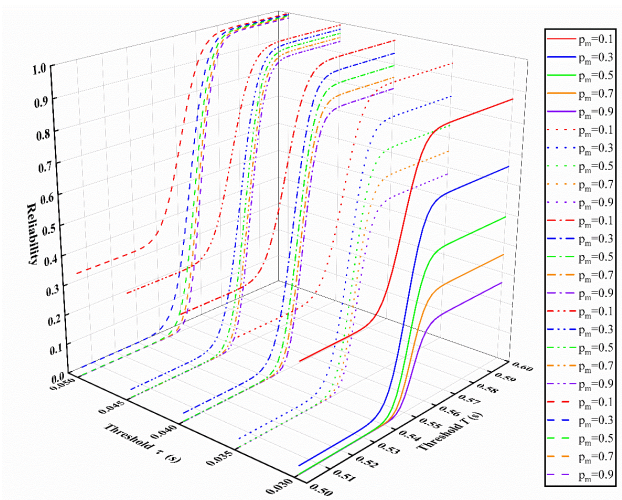


Fig. 15(e). Reliability curves with synchronization for different p_m

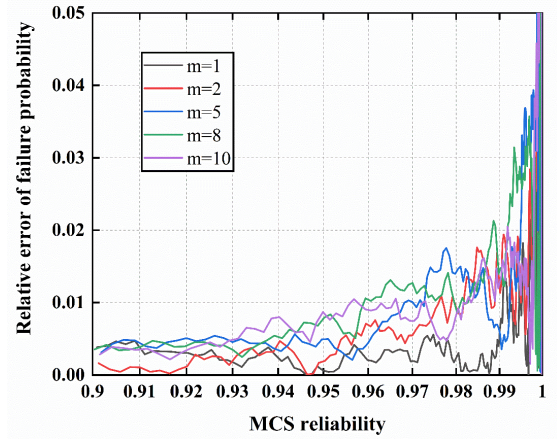


Fig. 15(f). Failure probability relative error without synchronization for Example 3.

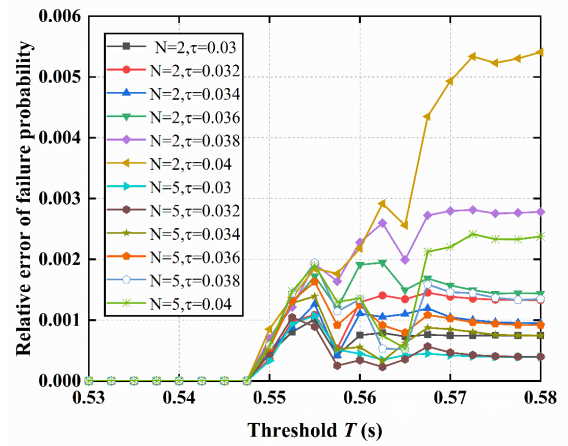


Fig. 15(g). Failure probability relative error with synchronization for Example 3.

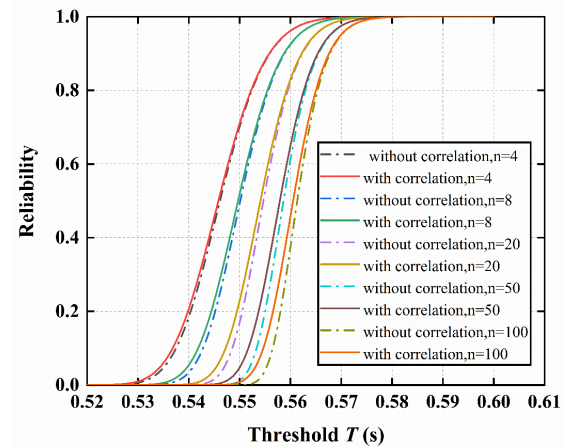


Fig. 15(h). Differences between the failure independent case and failure correlation for Example 3.

4.4. Reliability of deployment performance under mean value variations

This section assesses system reliability changes under varied mean values of random variables. The mean values listed in Table 8. Figure 16(a), 16(c), 16(e), 16(g) and 16(i) depict the

reliability without synchronization for V_q , δ , b_i , k_{di} and C_{ri} . Figure 16(b), 16(d), 16(f), 16(h) and 16(j) depict the reliability with synchronization and randomness of m for V_q , δ , b_i , k_{di} and C_{ri} .

Table 8. Mean values of random variables under different operating conditions.

Number	Random variable	Mean value	Number	Random variable	Mean value
1	V_q	100 (m/s)	6	b_i	8 (mm)
2	V_q	180 (m/s)	7	k_{di}	600 (N)
3	δ	30 (°)	8	k_{di}	500 (N)
4	δ	-30 (°)	9	C_{ri}	2 (mm)
5	b_i	6 (mm)	10	C_{ri}	1 (mm)

The synchronization threshold is denoted as τ ($\tau = 0.03, 0.035, 0.04, 0.045, 0.05$), p_m is set to 0.7, N_t is equal to 10. It can be seen that without considering synchronization and randomness of m , systems with the smaller mean value of V_q , larger mean value of δ , smaller mean value of b_i , larger mean value of k_{di} and larger mean value of C_{ri} exhibit higher reliability. When the means of the random variables change, the mean and dispersion of the system response will change. However, with the introduction of synchronization and randomness for m , during the ascending phase of the reliability curves (at the same τ), smaller mean values of V_q and b_i , and larger mean values of δ , k_{di} and C_{ri} , lead to higher system reliability. In the stable phase of the reliability curve (at the same τ), V_q , k_{di} and C_{ri} continue the change law of the reliability curve in the ascending phase, while the smaller mean value of δ results in the higher system reliability. For any given operating condition, as τ increases linearly, the reliability also increases, and the rate of increase diminishes gradually.

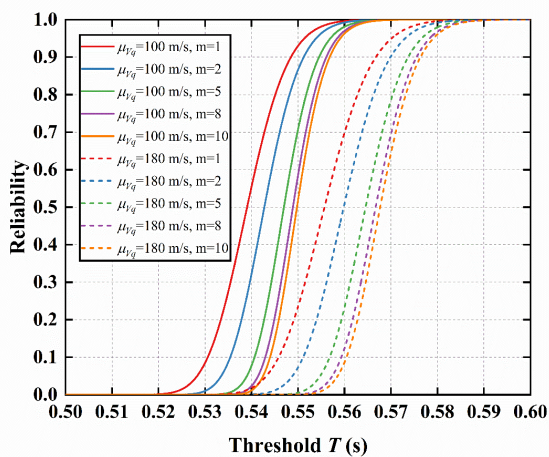


Fig. 16(a). Reliability curves without synchronization for conditions 1 and 2.

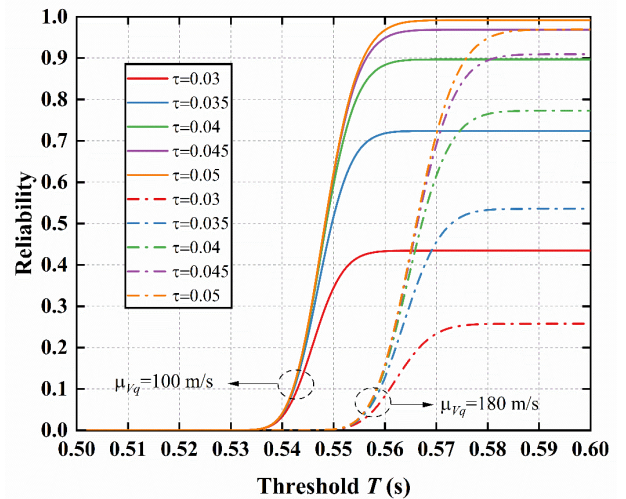


Fig. 16(b). Reliability curves considering both synchronization and randomness of m for conditions 1 and 2.

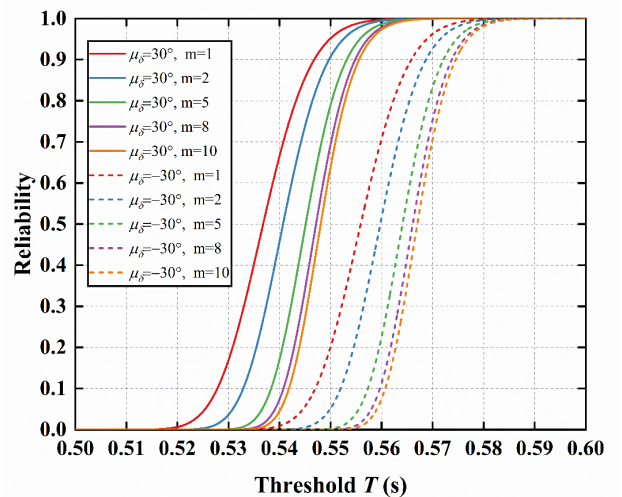


Fig. 16(c). Reliability curves without synchronization for conditions 3 and 4.

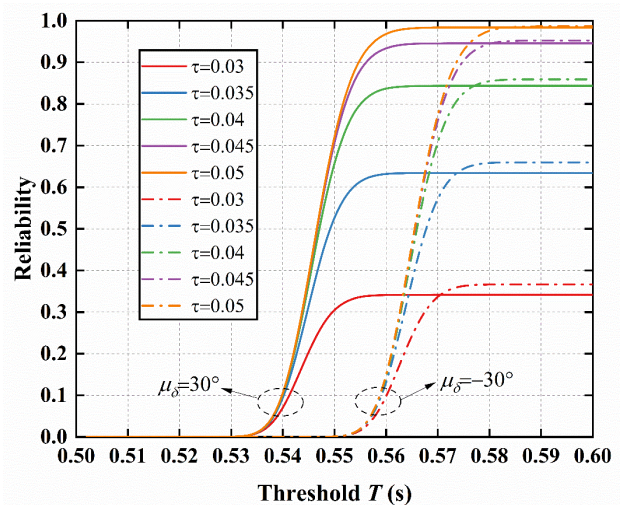


Fig. 16(d). Reliability curves considering both synchronization and randomness of m for conditions 3 and 4.

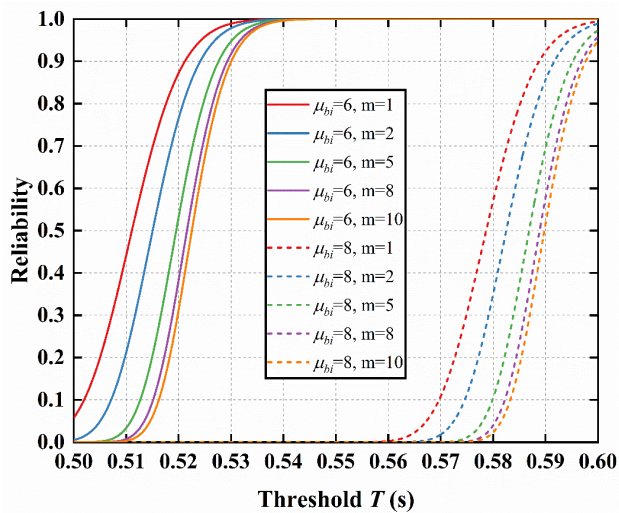


Fig. 16(e). Reliability curves without synchronization for conditions 5 and 6.

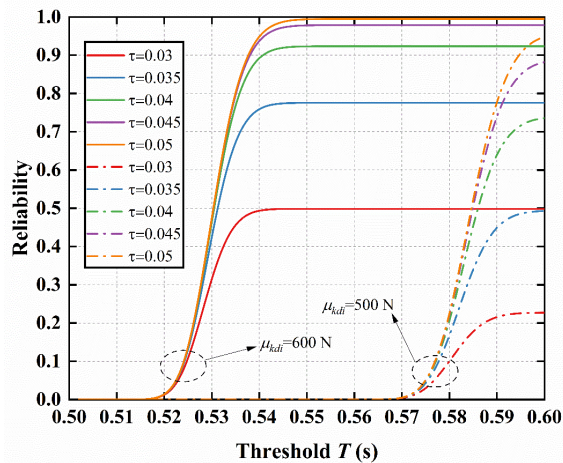


Fig. 16(h). Reliability curves considering both synchronization and randomness of m for conditions 7 and 8.

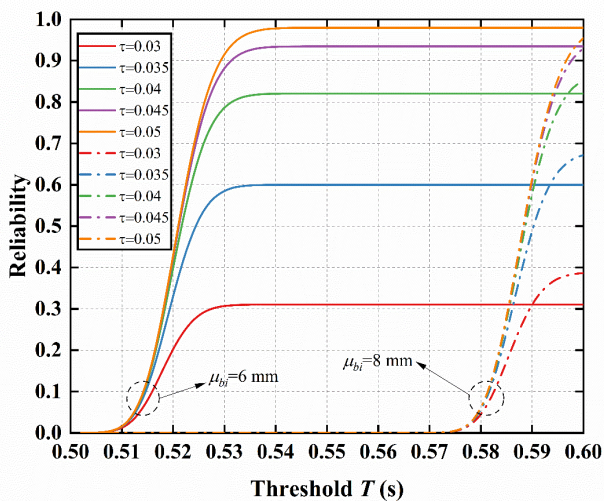


Fig. 16(f). Reliability curves considering both synchronization and randomness of m for conditions 5 and 6.

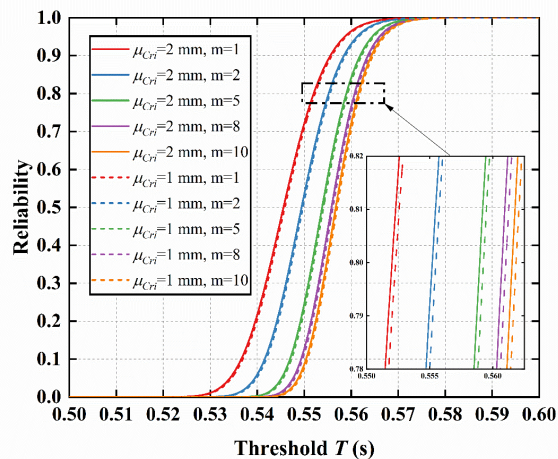


Fig. 16(i). Reliability curves without synchronization for conditions 9 and 10.

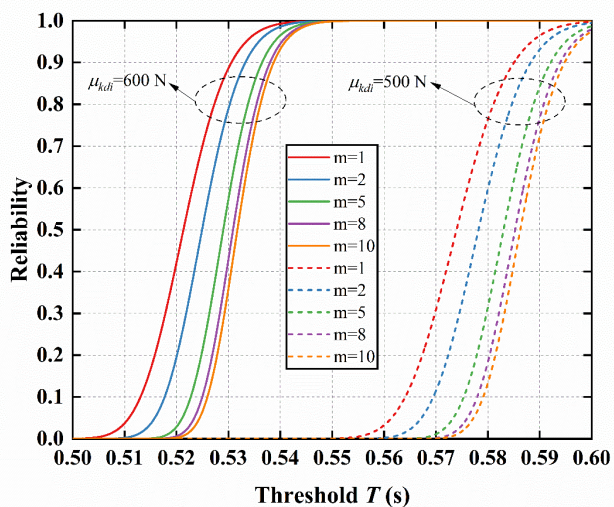


Fig. 16(g). Reliability curves without synchronization for conditions 7 and 8.

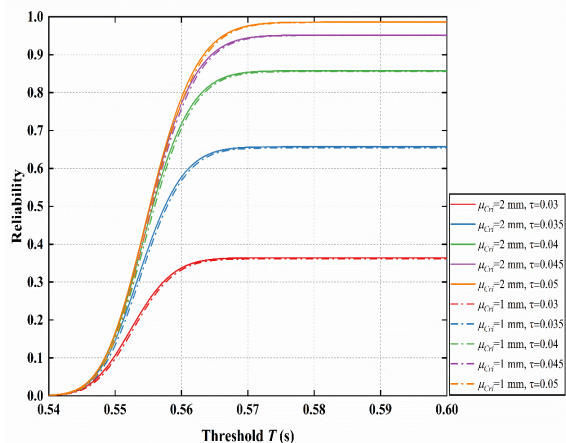


Fig. 16(j). Reliability curves considering both synchronization and randomness of m for conditions 9 and 10.

4.5. Reliability of deployment performance under standard deviation variations

This section primarily focuses on evaluating the system

reliability under different standard deviations. The standard deviations are presented in Table 9. Figure 17(a), 17(c), 17(e), 17(g) and 17(i) depict the reliability without synchronization for V_q , δ , b_i , k_{di} and C_{ri} . Figure 17(b), 17(d), 17(f), 17(h) and 17(j) depict the reliability with synchronization and randomness of m for V_q , δ , b_i , k_{di} and C_{ri} .

Table 9. Standard deviations of random variables under different operating conditions.

Number	Random variable	Standard deviation	Number	Random variable	Standard deviation
11	V_q	1 (m/s)	16	b_i	0.5 (mm)
12	V_q	20 (m/s)	17	k_{di}	1 (N)
13	δ	1 ($^\circ$)	18	k_{di}	30 (N)
14	δ	20 ($^\circ$)	19	C_{ri}	0.005 (mm)
15	b_i	0.01 (mm)	20	C_{ri}	0.2 (mm)

When the standard deviations of random variables change, both the dispersion and mean value of the system response will be affected. Without considering both synchronization and randomness of m , as T increases, the system reliability with smaller standard deviation for V_q , δ , b_i and k_{di} will gradually increase and surpass that with larger standard deviation. For C_{ri} , the reliability curves of both conditions are nearly coincident, and at the right boundary of T , the reliability is higher for the smaller standard deviation. As T increases, the difference in reliability, at any m level, always exhibits a pattern of “trough-peak-stabilization”. When considering both synchronization and randomness of m , at any τ level, the system reliability with the smaller standard deviation is always initially lower than the other, and then the former gradually increases and surpasses the latter. Moreover, near the right boundary of T , the system reliability with the smaller standard deviation is consistently higher than the other.

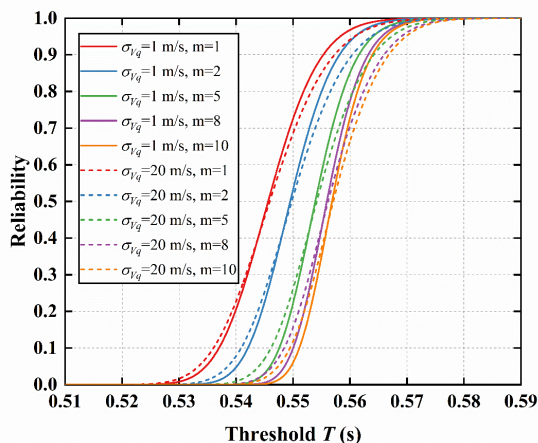


Fig. 17(a). Reliability curves without synchronization for conditions 11 and 12.

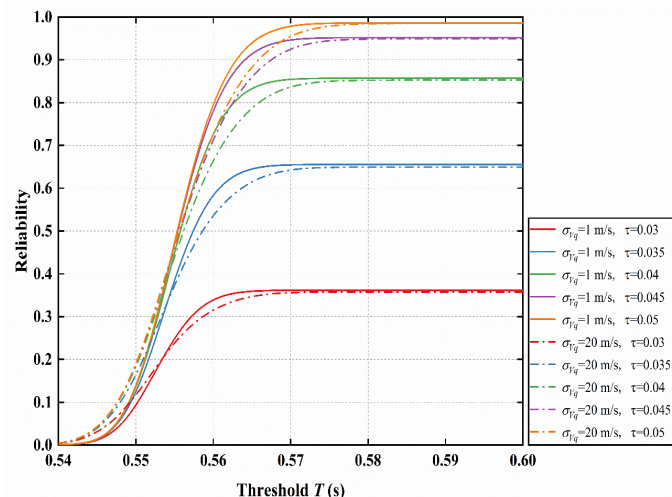


Fig. 17(b). Reliability curves considering both synchronization and randomness of m for conditions 11 and 12.

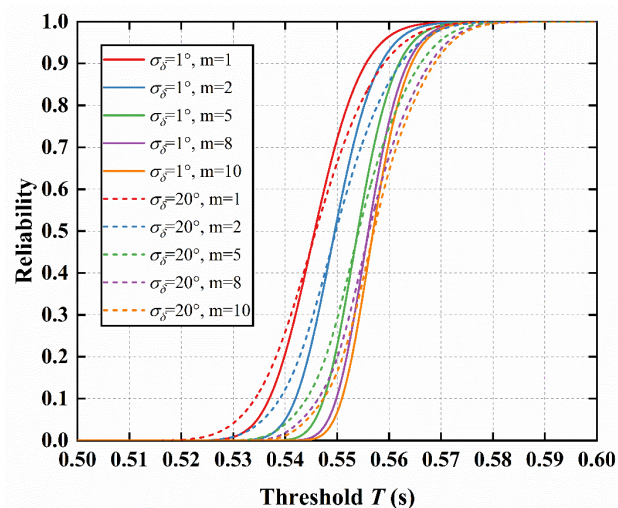


Fig. 17(c). Reliability curves without synchronization for conditions 13 and 14.

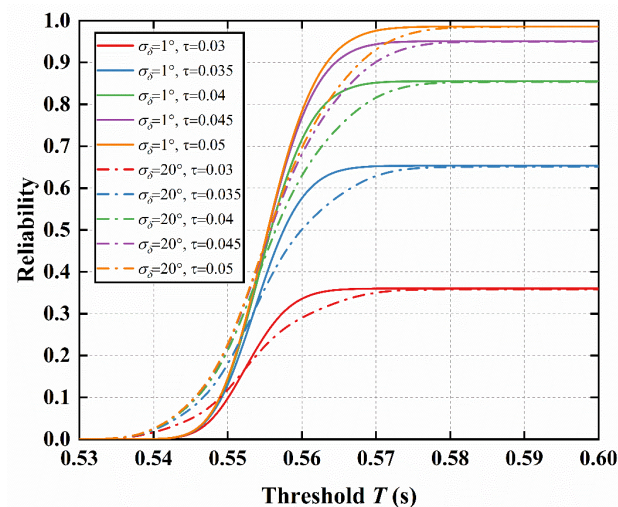


Fig. 17(d). Reliability curves considering both synchronization and randomness of m for conditions 13 and 14.

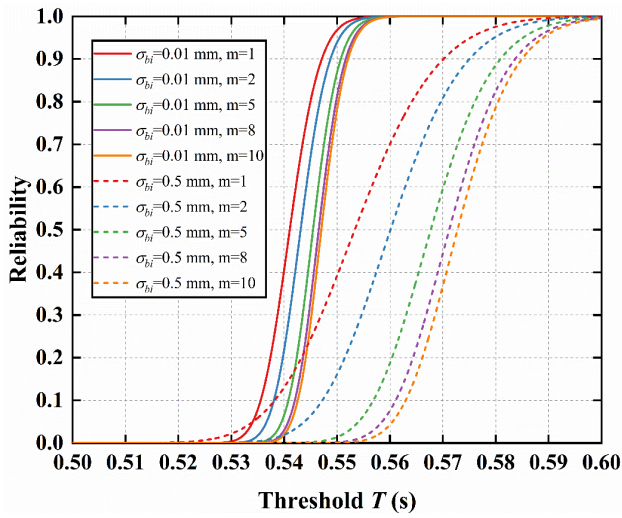


Fig. 17(e). Reliability curves without synchronization for conditions 15 and 16.

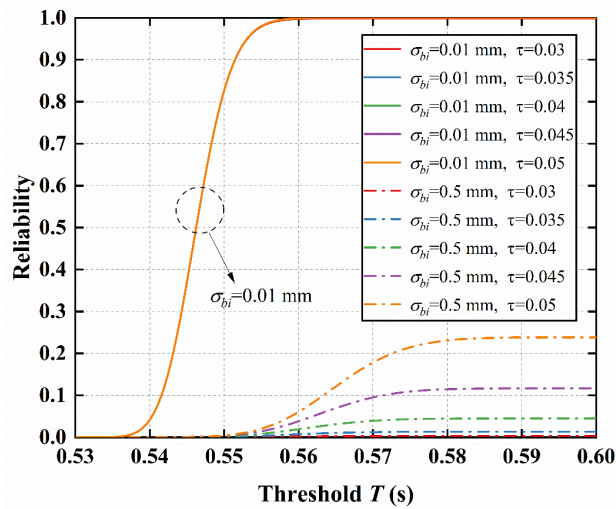


Fig. 17(f). Reliability curves considering both synchronization and randomness of m for conditions 15 and 16.

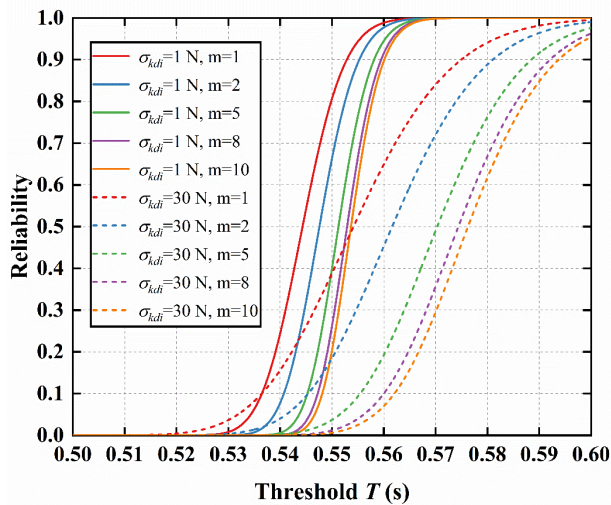


Fig. 17(g). Reliability curves without synchronization for conditions 17 and 18.

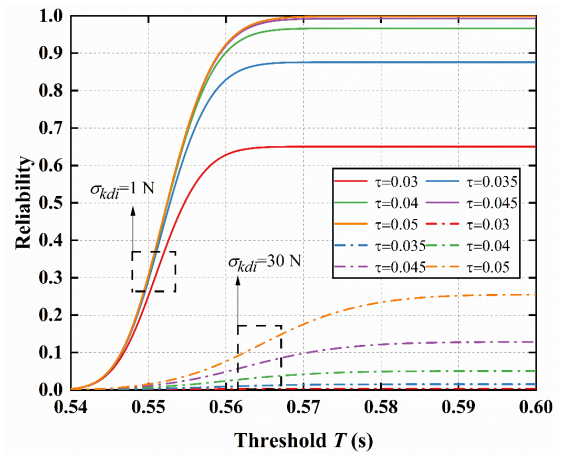


Fig. 17(h). Reliability curves considering both synchronization and randomness of m for conditions 17 and 18.

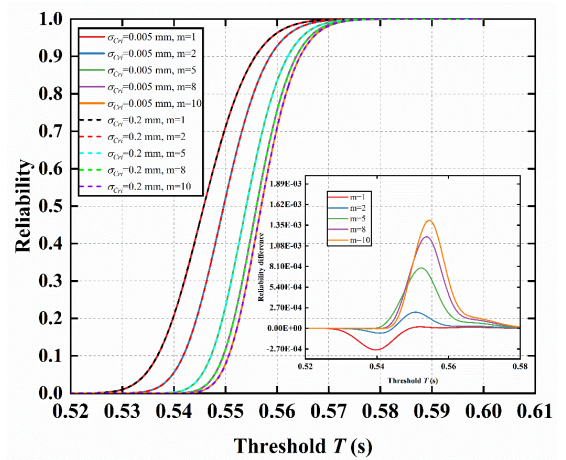


Fig. 17(i). Reliability curves without synchronization for conditions 19 and 20.

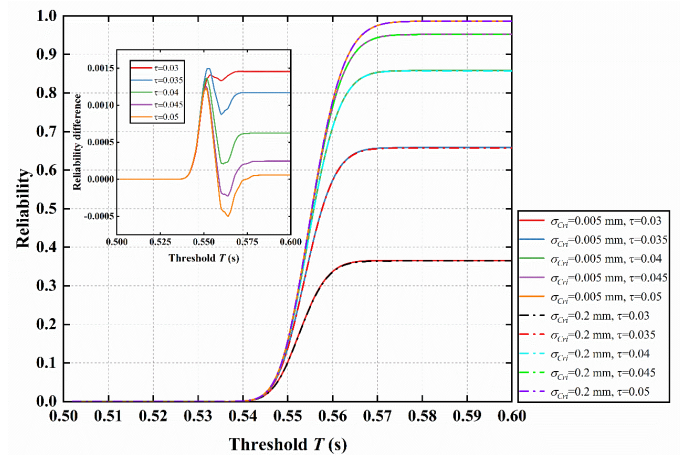


Fig. 17(j). Reliability curves considering both synchronization and randomness of m for conditions 19 and 20.

4.6 Deployment reliability considering randomness of crank and connecting rod lengths

In this example, the randomness of the crank and connecting rod lengths is taking into account. A total of 28,125 sample points

are computed. The distribution parameters of the random variables are listed in Table 10.

Table 10. Distribution parameters of random variables for folding wing system in example 6.

Parameter	Unit	Distribution	Mean value	Standard deviation
V_q	m/s	Normal	200	25
δ	°	Normal	0	25
$k_{d1}, k_{d2}, k_{d3}, k_{d4}$	N	Normal	1100	10
b_1, b_2, b_3, b_4	mm	Normal	6	0.25
$C_{r1}, C_{r2}, C_{r3}, C_{r4}$	mm	Normal	1.5	0.05
$l_{11}, l_{12}, l_{13}, l_{14}$	mm	Normal	1500	2
$l_{21}, l_{22}, l_{23}, l_{24}$	mm	Normal	1300	2

Figure 18(a) depicts the reliability under m ($m = 2, 5, 8, 10$) flight missions. As m increases, the reliability decreases. The case where synchronization is included is shown in Figure 18(b). It can be found that the reliability curves gradually remain in a stable state when T is greater than 0.47s. At a constant value of the number of deployments, the larger the τ is, the higher the reliability is. At a constant value of τ , the more the number of deployments, the lower the reliability. In addition, the final reliability difference between the two operating conditions gradually decreases as the τ grows. Obviously, these laws are consistent with the previous numerical examples.

The differences between the failure independent case and failure correlation case are shown in Figure 18(c). The standard deviations of the common cause random variables V_q and δ are 25. It is clear that the greater the dispersion of the common cause random variables, the greater the difference, the larger the error in the results under the assumption of independence. The other laws are the same as in Example 3.

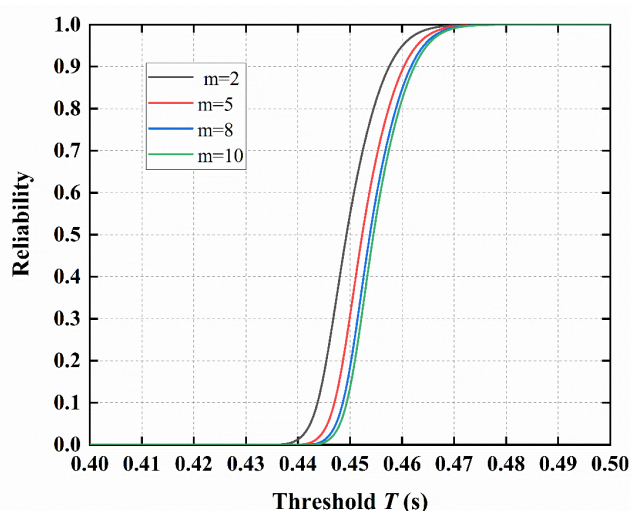


Fig. 18(a). Reliability curves without synchronization for $m > 1$.

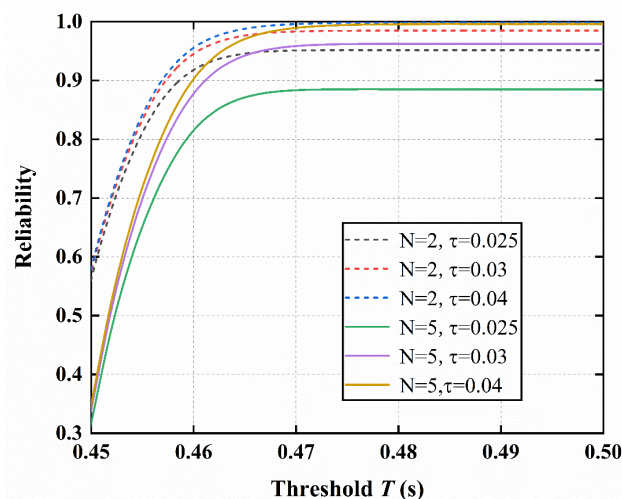


Fig. 18(b). Reliability curves with synchronization for multiple deployments.

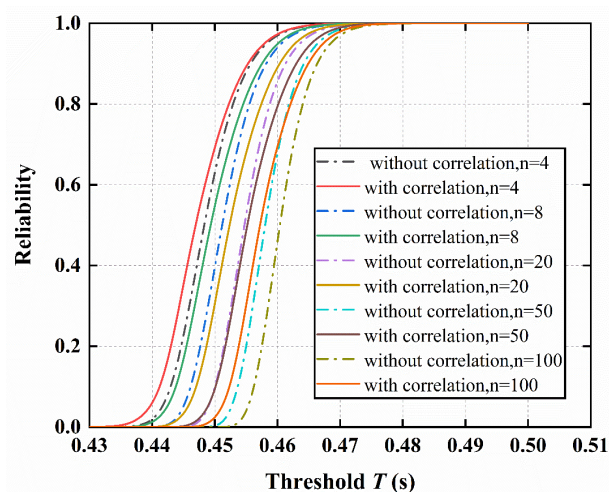


Fig. 18(c). Differences between the failure independent case and failure correlation for Example 6.

5. Conclusion

In this study, firstly, the dynamic model of the folding wing mechanism with joint clearances is established and solved. Subsequently, under the consideration of failure correlation, two reliability models for the deployment performance are developed: one without considering deployment synchronization and the other with deployment synchronization taken into account. Finally, the proposed methods are applied to solve the aforementioned reliability models, and their validity is verified through three illustrative examples. Additionally, an analysis of the system reliability variation under different distribution parameters of random variables is conducted. The conclusions are as follows:

1. The proposed methods are employed to calculate the first three cases. Remarkably, the results from MCS are found to be

in excellent agreement with the outcomes of the proposed method. Moreover, the proposed methods required significantly fewer samples to compute the system reliability. It is proved that the proposed methods have high efficiency, accuracy and universality in solving related system reliability problems.

2. From the numerical example of folding wing reliability analysis, it can be seen that the deployment time threshold, the synchronization threshold, the number of missions performed by the flight vehicle, and other parameters affect the reliability. And the degree of influence of each parameter on the reliability is different at different stages.

3. Regardless of whether the deployment synchronization is considered or not, when the random variable distribution parameters affecting the deployment time change, the deployment performance reliability of the folding wing system

also changes and is complicated. But there still exists the same rule of change.

4. In the series system of folding wing mechanism, the reliability obtained under the assumption of independence is more conservative compared to the case where failure dependence is considered. As the number of components in the system increases, the dispersion of common cause random variables increases, and the results under the assumption of independence deviate more from the true results.

In conclusion, the proposed methods can assess the system reliability of similar folding mechanisms efficiently and accurately. Moreover, from a reliability enhancement perspective, it offers valuable data support and guidance for the design, manufacturing and operational phases of such folding mechanisms.

Acknowledgement

All authors gratefully acknowledge the selfless support from the National Science and Technology Major Project (J2019-IV-0002-0069) and the Fundamental Research Funds for the Central Universities (N2303015). Thanks for the editor and reviewers.

Reference

1. Ambrósio J A C. Impact of rigid and flexible multibody systems: deformation description and contact models. *Virtual nonlinear multibody systems* 2003; 2: 57-81, https://doi.org/10.1007/978-94-010-0203-5_4.
2. Baumgarte J. Stabilization of constraints and integrals of motion in dynamical systems. *Computer methods in applied mechanics and engineering* 1972; 1: 1-16, [https://doi.org/10.1016/0045-7825\(72\)90018-7](https://doi.org/10.1016/0045-7825(72)90018-7).
3. Bucher C G, Bourgund U. A fast and efficient response surface approach for structural reliability problems. *Structural Safety* 1990; 7: 57-66, [https://doi.org/10.1016/0167-4730\(90\)90012-E](https://doi.org/10.1016/0167-4730(90)90012-E).
4. Chen J H, Chen L M, Qian L F, et al. Time-dependent kinematic reliability analysis of gear mechanism based on sequential decoupling strategy and saddle-point approximation. *Reliability Engineering & System Safety* 2022; 220: 108292, <https://doi.org/10.1016/j.ress.2021.108292>.
5. Chen X L, Wang T, Gao S. Dynamic response errors and accuracy reliability for mechanism with multiple lubrication clearance joints. *Archive of Applied Mechanics* 2023; 93: 525-550, <https://doi.org/10.1007/s00419-022-02283-2>.
6. Daniels H E. Saddlepoint approximations in statistics. *The Annals of Mathematical Statistics* 1954; 25: 631-650. <https://doi.org/10.1214/aoms/1177728652>
7. Fei C W, Li H, Liu H T, et al. Enhanced network learning model with intelligent operator for the motion reliability evaluation of flexible mechanism. *Aerospace Science and Technology* 2020; 107: 106342, <https://doi.org/10.1016/j.ast.2020.106342>.
8. Fleming K N, Mosleh A. Classification and analysis of reactor operating experience involving dependent events. Pickard, Lowe and Garrick, Inc., Newport Beach, CA (USA), 1985; No. EPRI-NP-3967.
9. Fleming K N. Reliability model for common mode failures in redundant safety systems. General Atomics 1974; <https://doi.org/10.2172/4206606>.
10. Flores P, Ambrósio J, Claro J C P, et al. A study on dynamics of mechanical systems including joints with clearance and lubrication. *Mechanism and Machine Theory* 2006; 41: 247-261, <https://doi.org/10.1016/j.mechmachtheory.2005.10.002>.
11. Flores P, Ambrósio J, Claro J C P. Kinematics and dynamics of multibody systems with imperfect joints: models and case studies. Springer Science & Business Media: 2008.
12. Gao Y, Hu M, Zhou X H, et al. Reliability evaluation for cable-spring folding wing considering synchronization of deployable mechanism.

- Actuators 2021; 10(5): 99, <https://doi.org/10.3390/act10050099>.
13. Guo F Y, Sun Z L, Zhang S N, et al. Optimal design and reliability analysis of a compliant stroke amplification mechanism. *Mechanism and Machine Theory* 2022; 171: 104748, <https://doi.org/10.1016/j.mechmachtheory.2022.104748>.
 14. Hasofer A M. An exact and invariant first order reliability format. *J. Eng. Mech. Div., Proc. ASCE*. 1974; 100: 111-121. <https://doi.org/10.1061/JMCEA3.0001848>
 15. Hauptmanns U. The multi-class binomial failure rate model. *Reliability Engineering & System Safety* 1996; 53: 85-90, [https://doi.org/10.1016/0951-8320\(96\)00025-7](https://doi.org/10.1016/0951-8320(96)00025-7).
 16. Huang B, Du X. Uncertainty analysis by dimension reduction integration and saddlepoint approximations. *Journal of Mechanical Design* 2006; 128: 26-33, <https://doi.org/10.1115/1.2118667>.
 17. Hurtado J E. Filtered importance sampling with support vector margin: a powerful method for structural reliability analysis. *Structural Safety* 2007; 29: 2-15, <https://doi.org/10.1016/j.strusafe.2005.12.002>.
 18. Kvam P H. A parametric mixture-model for common-cause failure data. *IEEE transactions on reliability* 1998; 47: 30-34, <https://doi.org/10.1109/24.690894>.
 19. Li G, He W X, Zeng Y. An improved maximum entropy method via fractional moments with Laplace transform for reliability analysis. *Structural and Multidisciplinary Optimization* 2019; 59: 1301-1320, <https://doi.org/10.1007/s00158-018-2129-6>.
 20. Li G, Zhang K. A combined reliability analysis approach with dimension reduction method and maximum entropy method. *Structural and Multidisciplinary Optimization* 2011; 43: 121-134, <https://doi.org/10.1007/s00158-010-0546-2>.
 21. Li J L, Yan S Z, Guo F, et al. Effects of damping, friction, gravity, and flexibility on the dynamic performance of a deployable mechanism with clearance. *Proceedings of the Institution of Mechanical Engineers, Part C: Journal of Mechanical Engineering Science* 2013; 227: 1791-1803, <https://doi.org/10.1177/0954406212469563>.
 22. Li X Y, Chen W B, Kang R. Performance margin-based reliability analysis for aircraft lock mechanism considering multi-source uncertainties and wear. *Reliability Engineering & System Safety* 2021; 205: 107234, <https://doi.org/10.1016/j.res.2020.107234>.
 23. Li Y Y, Wang C, Huang W H. Dynamics analysis of planar rigid-flexible coupling deployable solar array system with multiple revolute clearance joints. *Mechanical Systems and Signal Processing* 2019; 117: 188-209, <https://doi.org/10.1016/j.ymsp.2018.07.037>.
 24. Li Y Y, Yang Y, Li M, et al. Dynamics analysis and wear prediction of rigid-flexible coupling deployable solar array system with clearance joints considering solid lubrication. *Mechanical Systems and Signal Processing* 2022; 162: 108059, <https://doi.org/10.1016/j.ymsp.2021.108059>.
 25. Mallor C, Calvo S, Núñez J L, et al. On the use of probabilistic fatigue life estimation in defining inspection intervals for railway axles. *Procedia Structural Integrity* 2021; 33: 391-401, <https://doi.org/10.1016/j.prostr.2021.10.047>.
 26. Marshall, Albert W, Olkin I. A multivariate exponential distribution. *Journal of the American Statistical Association* 1967; 62: 30-44, <https://doi.org/10.1080/01621459.1967.10482885>.
 27. Mosleh A. A multi-parameter event based common-cause failure model. *SMiRT9 Paper* 1987; No. M7/3.
 28. Mukras S, Kim N H, Mauntler N A, et al. Analysis of planar multibody systems with revolute joint wear. *Wear* 2012; 268: 643-652, <https://doi.org/10.1016/j.wear.2009.10.014>.
 29. Pang H, Shi D Y, Wang D C. Research on mission reliability and sensitivity of folding tail mechanism. *IOP Conference Series: Materials Science and Engineering* 2021; 1043: 052018, <https://doi.org/10.1088/1757-899X/1043/5/052018>.
 30. Pang H, Yu T X, Wang N. Synchronization reliability evaluation method for mechanisms with different time distribution. *Mathematical Problems in Engineering* 2018; <https://doi.org/10.1155/2018/8756975>.
 31. Vaurio J K. Availability of redundant safety systems with common-mode and undetected failures. *Nuclear Engineering and Design* 1980; 58: 415-424, [https://doi.org/10.1016/0029-5493\(80\)90154-5](https://doi.org/10.1016/0029-5493(80)90154-5).
 32. Wang B W, Xie L Y, Fan F Y, et al. Reliability analysis of folding wing deployable mechanism considering common cause failure. *Journal of Mechanical Engineering* 2020; 56(5): 161-170, <https://doi.org/10.3901/JME.2020.05.161>.
 33. Wang L, Zhang X F, Zhou Y J J. An effective approach for kinematic reliability analysis of steering mechanisms. *Reliability Engineering & System Safety* 2018; 180: 62-76, <https://doi.org/10.1016/j.res.2018.07.009>.
 34. Wang W, Shen G, Zhang Y M, et al. Dynamic reliability analysis of mechanical system with wear and vibration failure modes. *Mechanism and Machine Theory* 2021; 163: 104385, <https://doi.org/10.1016/j.mechmachtheory.2021.104385>.

35. Xie L Y, Lin W Q. Control parameters and quantification for system reliability design. *Materials Science Forum* 2009; 628: 215-220, <https://doi.org/10.4028/www.scientific.net/MSF.628-629.215>.
36. Zhang C Y, Bai G C. Extremum response surface method of reliability analysis on two-link flexible robot manipulator. *Journal of Central South University* 2012; 19: 101-107, <https://doi.org/10.1007/s11771-012-0978-5>.
37. Zhang J F, Du X P. Time-dependent reliability analysis for function generation mechanisms with random joint clearances. *Mechanism and Machine Theory* 2015; 92: 184-199, <https://doi.org/10.1016/j.mechmachtheory.2015.04.020>.
38. Zhang P, Hu X Z, Sun H L. Reliability vector methods for series and parallel engineering systems under failure dependence. *Journal of Sichuan University* 2004; 1: 1-6.
39. Zhao H B. Slope reliability analysis using a support vector machine. *Computers and Geotechnics* 2008; 35: 459-467, <https://doi.org/10.1016/j.compgeo.2007.08.002>.
40. Zhao Y G, Ang A. System reliability assessment by method of moments. *Journal of Structural Engineering* 2003; 129(10): 1341-1349, [https://doi.org/10.1061/\(ASCE\)0733-9445\(2003\)129:10\(1341\)](https://doi.org/10.1061/(ASCE)0733-9445(2003)129:10(1341)).
41. Zhao Y G, Lu Z H. Applicable range of the fourth-moment method for structural reliability. *Journal of Asian Architecture and Building Engineering* 2007; 6(1): 151-158, <https://doi.org/10.3130/jaabe.6.151>.
42. Zhao Y G, Ono T. On the problems of the fourth moment method. *Structural Safety* 2004; 26(3): 343-347, <https://doi.org/10.1016/j.strusafe.2003.10.001>.
43. Zheng E L, Wang T Y, Guo J, et al. Dynamic modeling and error analysis of planar flexible multilink mechanism with clearance and spindle-bearing structure. *Mechanism and Machine Theory* 2019; 131: 234-260, <https://doi.org/10.1016/j.mechmachtheory.2018.09.023>.
44. Zhou C C, Zhao H D, Chang Q, et al. Reliability and global sensitivity analysis for an airplane slat mechanism considering wear degradation. *Chinese Journal of Aeronautics* 2021; 34: 163-170, <https://doi.org/10.1016/j.cja.2020.09.048>.
45. Zhou D, Pan E S, Zhang X F, et al. Dynamic model-based saddle-point approximation for reliability and reliability-based sensitivity analysis. *Reliability Engineering & System Safety* 2020; 201: 106972, <https://doi.org/10.1016/j.res.2020.106972>.
46. Zhou D, Zhang X F, Zhang Y M. Dynamic reliability analysis for planetary gear system in shearer mechanisms. *Mechanism and Machine Theory* 2016; 105: 244-259, <https://doi.org/10.1016/j.mechmachtheory.2016.07.007>.
47. Zhuang X C, Yu T X, Liu J Y, et al. Kinematic reliability evaluation of high-precision planar mechanisms experiencing non-uniform wear in revolute joints. *Mechanical Systems and Signal Processing* 2022; 169: 108748, <https://doi.org/10.1016/j.ymsp.2021.108748>.
48. Zhuang X C, Yu T X, Shen L J, et al. Time-varying dependence research on wear of revolute joints and reliability evaluation of a lock mechanism. *Engineering Failure Analysis* 2019; 96: 543-561, <https://doi.org/10.1016/j.engfailanal.2018.10.017>.

Nomenclature

$\mathbf{r}_j, \mathbf{r}_i$	the generalized coordinates of the center of mass for the journal and the bearing components
$\mathbf{A}_j, \mathbf{A}_i$	the transformation matrices for the journal and bearing components
$\mathbf{s}_j^c, \mathbf{s}_i^c$	the position vectors of the journal and bearing centers in the local coordinate system
\mathbf{n}, \mathbf{t}	unit normal vector and unit tangent vector
Δ	penetration depth
C_r	clearance size
C_r^B, C_r^C	the clearance sizes of joint B and joint C
$\dot{\mathbf{r}}_j^Q, \dot{\mathbf{r}}_i^Q$	The velocities of contact points for the journal and bearing
v_n, v_t	The normal and tangential projections of the relative contact velocity
C_e	restitution coefficient
K	stiffness coefficient
F_N, F_T	the normal contact force and friction force
$\mathbf{F}_j, \mathbf{F}_i$	the contact resultant forces for the bearing and journal components
M_j^c, M_i^c	the moments for the bearing and journal components
k_d	the peak of the driving force
ρ_a	air density
C_0	air drag coefficient
b_1, b_2	the thickness of the main wing and auxiliary wing

l_1, l_2	the lengths of the main wing and auxiliary wing
V_q	flight speed
δ	pitch angle
w_1, w_2	the widths of the main wing and auxiliary wing
V_3	the volume of the slider
ρ_1, ρ_2, ρ_3	the densities of the main wing, auxiliary wing, and slider
E_1, E_2	Elastic modulus of aluminum alloy and steel
ν_1, ν_2	Poisson's ratio of aluminum alloy and steel
c_f	friction coefficient
c	the distance between the slider and X-axis
R_1^b, R_2^b	bearing inner radii at joint B and joint C
$t_i (i = 1, 2, 3, 4)$	the actual deployment time for the i th set of folding wing
$R_i (i = 1, 2, 3, 4)$	the deployment performance reliability for the i th set of folding wing
$R_{s V_q, \delta}$	the system conditional reliability when V_q and δ are constant values
$t_{i V_q, \delta}$	the deployment time of i th set of folding wing when V_q and δ are fixed
R_s	the system reliability
$H_{t_i V_q, \delta}(t_i V_q, \delta)$	the conditional cumulative distribution function of $t_{i V_q, \delta}$
R_s^*	the system reliability with synchronization
$R_{s V_q, \delta}^{*m}$	the system conditional reliability for m flight missions when V_q and δ are fixed with synchronization
R_s^{*m}	the system conditional reliability for m flight missions with synchronization
$\hat{h}_{i V_q, \delta}(t_i V_q, \delta)$	the approximate probability density function of $t_{i V_q, \delta}$